JMBFS

Journal of Microbiology, Biotechnology and Food Sciences

International peer-reviewed scientific online journal

Published by Faculty of Biotechnology and Food Sciences

# MOLECULAR DYNAMICS ANALYSIS REVEALED THE ENHANCED STABILITY AND SPECIFICITY OF SCFV-CYTOKINE COMPLEXES TARGETING PRIMARY TARGETS

*Kumar Simant and Krishnan Venkataraman* *

***Address(es):***
[1] Centre for Bio-Separation Technology (CBST), Vellore Institute of Technology (VIT), Vellore – 632014, India.

*Corresponding author: krishnan.v@vit.ac.in

https://doi.org/10.55251/jmbfs.12997

ARTICLE INFO

Received 30. 6. 2025
Revised 28. 4. 2026
Accepted 29. 4. 2026
Published 1. 6. 2026

Regular article

OPEN ACCESS

**ABSTRACT**

Single-chain variable fragments (scFvs) are promising alternatives to full-length monoclonal antibodies because of their small size, high specificity, and improved tissue penetration. However, potential cross-reactivity with structurally related proteins may limit their therapeutic applicability. In the present study, an in-silico workflow integrating protein structure prediction, protein–protein docking, and molecular dynamics (MD) simulations were employed to evaluate the binding specificity and structural stability of murine anti-IL-6 scFv and anti-TNF-α scFv toward their primary cytokine targets and related off-target cytokines. Predicted scFv structures were docked with IL-6, IL-11, TNF-α, and TNF-β, followed by 200ns MD simulations of the resulting complexes. Comparative analyses were performed using root mean square deviation (RMSD), root mean square fluctuation (RMSF), radius of gyration (Rg), solvent-accessible surface area (SASA), and hydrogen-bonding profiles. Complexes formed with the primary targets showed lower structural deviation and greater conformational stability than cross-reactive complexes. The anti-IL-6 scFv–IL-6 and anti-TNF-α scFv–TNF-α systems exhibited lower average RMSD values than their corresponding control complexes with IL-11 and TNF-β. In addition, primary target complexes demonstrated more stable intermolecular interactions, improved compactness, and reduced residue-level fluctuations at key binding regions. Molecular Mechanics Poisson-Boltzmann Surface Area (MM-PBSA) analysis suggested that the scFv showed more efficient binding with its primary target. Overall, these findings suggest that the studied scFvs displayed preferential binding and enhanced dynamic stability toward their intended cytokine targets. These computational studies may provide a structural basis for future experimental validation and rational engineering of antibody fragments which targets the respective cytokines. Both TNF-α and IL-6 are important cytokines, and their levels are elevated in many chronic diseases. Blocking them looks like a promising way to treat these diseases and blocking their activities by scFv may provide alternative ways to treat these diseases.

**Keywords:** monoclonal antibody (mAb), single-chain variable fragment (scFv), protein-protein docking, IL-6, TNF-α, antibody engineering

## INTRODUCTION

Monoclonal antibody (mAb) therapeutics have gained prominence as leading biopharmaceuticals due to their unparalleled specificity, adaptability, and clinical success across various medical conditions. Their popularity stems from their ability to precisely target disease-specific antigens while leaving healthy tissues, minimising off-target effects **(Scott *et al.*, 2012)**. For instance, in oncology, mAbs like trastuzumab (anti-HER2) exploit antibody-dependent cellular cytotoxicity (ADCC) to selectively eliminate HER-2 positive breast cancer cells, significantly improving survival rates compared with traditional chemotherapy **(Scott *et al.*, 2012)**. These advances have been further expanded through antibody engineering approaches, exemplified by bispecific antibodies such as blinatumomab, which simultaneously binds the tumour antigen CD19 and the T-cell receptor CD3, thereby redirecting T cells to eliminate malignant B cells in acute lymphoblastic leukaemia. **(Kantarjian *et al.*, 2017)**.

The structural and functional versatility of mAbs has been significantly expanded through the development of various antibody fragments. These engineered constructs retain the target-binding capabilities of conventional antibodies while offering distinct advantages such as tissue penetration, production efficiency, and adaptability for specific therapeutic applications **(Holliger & Hudson, 2005)**. The basic antibody fragments have been refined through various engineering approaches to enhance their properties for specific applications such as Fab, single-chain variable fragment (scFv) and single-domain antibody (sdAb), which offer distinct advantages over full-length antibodies due to their smaller size, enhanced tissue penetration, and reduced immunogenicity. Fab fragments comprise one antigen-binding domain linked by a disulfide bond. These fragments lack the Fc region **(Bridger *et al.*, 1996; Zhang *et al.*, 2023)**. sdAbs are derived from heavy-chain antibodies that retain high antigen affinity despite their minimal size **(Muyldermans, 2013)**. The generation of antibodies generally employs phage display technology, which facilitates the production of either a single-chain variable fragment (scFv), which comprises a short peptide linker that connects the variable heavy (VH) and light chains (VL), or an antigen-binding fragment (Fab). This structure allows the efficient expression of scFv antibodies in the functional form in *E. coli*, facilitating protein engineering to enhance their affinity and modify their specificity **(Muñoz-López *et al.*, 2022)**. Numerous scFv antibodies have been developed against various targets, including haptens **(Kobayashi *et al.*, 2005)**, proteins **(Dai *et al.*, 2003)**, carbohydrates **(Ravn *et al.*, 2004)**, receptors **(Galeffi *et al.*, 2006)**, tumor antigens **(He *et al.*, 2002)**, and viruses. Due to their high specificity and adaptability, scFv antibodies have significant potential for applications in medical therapies and diagnostic technologies **(Ahmad *et al.*, 2012)**. However, these antibody fragments typically require further molecular engineering and expression in appropriate host systems before being converted into fully functional antibodies **(Green, 1999)**.

A major application of scFv antibodies is to modulate immune responses, particularly in pathological states where excessive immune activation occurs, such as cytokine storms **(Xue *et al.*, 2021)**. A cytokine storm is triggered predominantly by an uncontrolled overproduction of pro-inflammatory cytokines, resulting in systemic inflammation, tissue injury and, in severe instances, multi-organ failure. scFv antibodies, being small, with high specificity and manageable engineering processes, demonstrate propitious therapeutic promises in targeting and neutralizing important cytokines involved in hyper-inflammation **(Simant & Venkataraman, 2022)**. The design of scFv antibodies for cytokines such as IL-6 and TNF-α aims at the regulation of immune overactivation, thereby conceiving therapeutic approaches for sepsis, acute respiratory distress syndrome (ARDS), and severe viral infections, including COVID-19 **(Hu *et al.*, 2021; Yiu *et al.*, 2012)**.

scFv antibody engineering for cytokine storm has been greatly facilitated by bioinformatics strategies, enabling antibody design, optimization, and interaction modelling **(Yaghoobizadeh *et al.*, 2024)**. Computational methodologies like structure prediction, molecular docking and artificial intelligence-based molecular dynamic simulation play key roles in enhancing the stability, affinity, and specificity of scFv against proinflammatory cytokines such as IL-6 and TNF-α. Bioinformatics-guided analysis also anticipates immunogenicity, so engineered antibodies reduce unwanted immune responses in therapeutic use **(Ayub *et al.*, 2023; Srivastava *et al.*, 2021)**. These integrative tools address the gap between experimental antibody engineering and computational immunology, accelerating

the discovery of next-generation Immunotherapeutics **(Khetan *et al.*, 2022)**. The combination of computational tools and antibody informatics optimizes the rational antibody design, thereby facilitating discovery to the clinical pathway **(Jarasch *et al.*, 2015; Khetan *et al.*, 2022)**.

The inclusion of computational analysis within the context of antibody drug discovery is in alignment with the objectives of this study, which seek to optimize scFv antibodies, and check their stability and cross-reactivity through structure-based strategies. By applying homology modelling for structure prediction, this study seeks to accurately reconstruct the three-dimensional structures of anti-IL-6 scFv and anti-TNF-α scFv antibodies, thus paving the way for subsequent analysis **(Safarpour *et al.*, 2018)**. The identification of complementarity-determining regions (CDRs) allows for the determination of antigen-binding specificity, which in turn guides targeted engineering efforts to optimize binding affinity and stability. Protein-protein docking will enable the exploration of scFv antibody-cytokine target interactions, whereas molecular dynamics (MD) simulations will guide the stability and conformational flexibility of docked complexes under physiological conditions. Through the integration of these computational methods, this study aimed to optimize scFv antibody leads to enhance their therapeutic utility, ultimately laying the groundwork for the development of targeted and effective therapies for cytokine-mediated diseases.

## MATERIALS AND METHODS

### Protein structure prediction

The cloned sequence of murine anti-IL-6 scFv and anti-TNF-α scFv was obtained from Prof. M.A. Vijayalakshmi (Founder, Centre for Bio-Separation Technology, VIT, Vellore) which was primarily developed by her. Due to the novel nature of anti-IL-6 scFv and anti-TNF-α scFv and the PDB structure is not available as the three-dimensional structures have not been elucidated. Therefore, protein structure prediction was performed. The amino acid sequence of the protein (see supplementary data) was subjected to various protein structure prediction tools such as the SwissModel (RRID:SCR_018123) **(Guex *et al.*, 2009; Waterhouse *et al.*, 2018)**, Iterative Threading ASSEmbly Refinement (i-TASSER) (RRID:SCR_014627) **(Yang & Zhang, 2015; Zhou *et al.*, 2022)**, Phyre2.2 (RRID:SCR_010270) **(Powell *et al.*, 2025)**, and AlphaFold3 server (RRID:SCR_025885) **(Abramson *et al.*, 2024)** developed by Google DeepMind. The SwissModel is an automated tool that identifies suitable templates based on sequence similarity using protein data bank (PDB). The most reliable model was selected based on global model quality estimation (GMQE) and QMEAN scores. In the case of i-TASSER, this tool generated multiple protein models through thread-based modelling and fragment assembly simulations. Phyre2.2 is the tool that uses both homology modelling and ab initio structure prediction. The most capable structure was determined based on the confidence score. Last, AlphaFold3, a deep-learning based protein prediction model, was used. The sequence was submitted to AlphaFold3, and the predicted structure was ranked based on the predicted local-distance difference test (pLDDT) scores. Out of all the tools the best model was taken forward for the study, which was selected based on the ERRAT overall quality scores and PROCHECK **(Laskowski *et al.*, 1993, 1996)** results, which was obtained from SAVES v6.1 server (RRID:SCR_018219) **(Colovos & Yeates, 1993)** provided by the University of California, Los Angeles (UCLA).

### Identification of Complementarity Determining Regions (CDRs)

The amino acid sequences of both proteins were subjected to "SAbPred: ABodyBuilder2" (RRID:SCR_022094), which is a sophisticated tool that was developed by Oxford Protein Informatics Groups (OPIG) **(Dunbar *et al.*, 2016)**. ABodyBuilder2 is one of the most accurate means to predict CDR structure where the heavy and light chain sequences were fed to the server and a numbering system was used on default i.e., IMGT **(Abanades *et al.*, 2023)**.

### Preparation of cytokine structures

Experimentally resolved cytokine structures used as docking partners were retrieved from the Protein Data Bank. The following structures were used which were docked with anti-IL-6 scFv and TNF-α scFv.

- Human IL-6: PDB ID: 1ALU
- Human IL-11: PDB ID: 6O4O
- Human TNF-α: PDB ID: 1TNF
- Human TNF-β: PBD ID: 1TNR

Prior to docking, all cytokine structures were inspected and prepared by removing non-essential heteroatoms, solvent molecules, and crystallographic artefacts where applicable. Missing hydrogen atoms were added, and structures were subjected to energy minimization using YASARA server before downstream analysis.

### Molecular docking of scFv in various combinations

Molecular protein-protein docking was carried out using HADDOCKv2.4 (High Ambiguity Driven protein-protein DOCKing) server (RRID:SCR_019091) developed by Bonvin lab at Utrecht University, Nederland **(Honorato *et al.*, 2021, 2024)**. Before subjecting the chosen protein models to docking, the energy minimization step was performed using the free YASARA energy minimization server (RRID:SCR_017591) **(Krieger *et al.*, 2009)**. After minimization, the predicted models were processed by the HADDOCKv2.4 server. Then, the active residues were selected for both the proteins that were directly involved in the interaction i.e. CDRs in this case. After marking all other parameters as default, the job was submitted. The combinations in which docking was performed are listed in Table 1. These combinations were performed to address the specificity of each scFv to its primary target and potential cross-reactivity with structurally related cytokines. The interactions and H-bond analysis was performed using ChimeraXv1.9 (RRID:SCR_015872) **(Goddard *et al.*, 2005, 2018; Pettersen *et al.*, 2021)**, which is an emerging generation molecular visualization software, developed by UCSF (University of California, San Francisco) with the support of the National Institute of Health (USA), Chan Zukerberg initiative and National Institute of allergy and infectious diseases (USA).

**Table 1** Various combinations in which docking was performed using HADDOCK v2.4

| S. No. | Molecule 1 | Molecule 2 |
|---|---|---|
| **1** | Murine anti-IL-6 scFv | Human IL-6 |
| **2** | Murine anti-IL-6 scFv | Human IL-11 |
| **3** | Murine anti-TNF-α scFv | Human TNF-α |
| **4** | Murine anti-TNF-α scFv | Human TNF-β |

### Molecular Dynamic (MD) simulation

The MD simulations were performed for the docked complexes obtained from HADDOCKv2.4. The method was executed to determine the relative stability and conformational changes of the complexes in an artificially simulated solvated system **(Abraham *et al.*, 2015)**. The simulation was performed using the GROMACS (RRID:SCR_014565) simulation package to perform fully solvated molecular dynamic simulations **(Abraham *et al.*, 2015; Lindahl *et al.*, 2010)**. For the simulation, the PDB file of the docked complex was uploaded and was performed by applying CHARMM36M force field. The complex was solvated in a cubic box with a transferable intermolecular potential of 3 points (TIP3P) water model. Neutralization of the solvent system was performed by adding 0.15 M NaCl. Prior to the simulation, energy minimization was performed for the system implementing the steepest descent as an integrator for 5000 steps. The system was then equilibrated by an NVT/NPT (where, N, number of particles; V, volume; T, temperature and P, pressure) module with temperature at 310K and pressure at 1 bar **(Thomas & Satija, 2024)**. The simulation was further performed for 200 ns with a leap-frog MD integrator at 1000 frames per simulation **(Debroy *et al.*, 2023; Thomas *et al.*, 2024)**. The simulation results were calculated in the form of root mean square deviation (RMSD) of the given structure over time, root mean square fluctuation (RMSF) of each residue of the given structure, radius of gyration (Rg) or structural compactness, solvent accessible surface area (SASA), and average number of hydrogen bonds in each frame over time.

### Binding energy analysis

To quantitatively evaluate the binding affinity of the scFv construct toward the target cytokine, Molecular Mechanics Poisson-Boltzmann Surface Area (MM-PBSA) analysis was employed as a post-processing free energy estimation approach. MM-PBSA is a well-established and widely validated free energy methodology that offers a rational balance among computational tractability and predictive accuracy of ligand and receptor binding energies within the framework of structure-based therapeutic design **(Genheden & Ryde, 2015)**. In the present study, MM-PBSA calculations were rigorously carried out utilizing the gmx_MMPBSA (v1.5.0.3) toolkit, which interfaces seamlessly with the MMPBSA.py (v16.0) module and operates within the GROMACS computational environment.

## RESULTS AND DISCUSSIONS

### Protein structure prediction

The 3D structures of both scFv antibodies were predicted using four computational tools as mentioned in section 0. These tools were selected to leverage their unique approaches for structure prediction, which is template-based modelling in case of Phyre2 and SwissModel, threading and ab-initio modelling in case of i-TASSER and deep-learning based structure prediction in case of AlphaFold. Belatedly, the models were evaluated for the quality and reliability for further processes.

The quality of the predicted structures was determined by uploading the PDB files of the structures on the SAVES server, which gives the ERRAT quality score and Ramachandran plot from the PROCHECK server.

**Structural models and visual comparisons**

The predicted structures from each tool showed varying degrees of similarity in their overall fold, with the characteristic β-sheet structure, typical of immunoglobulin variable domains. **Figure** 0.1 shows the superimposed structures of the models generated by i-TASSER, Phyre2, SwissModel and AlphaFold. The results highlight the differences in all the structures, particularly in the linker region. The visible differences in the structures can be primarily due to the differences in template selection and modelling algorithms.

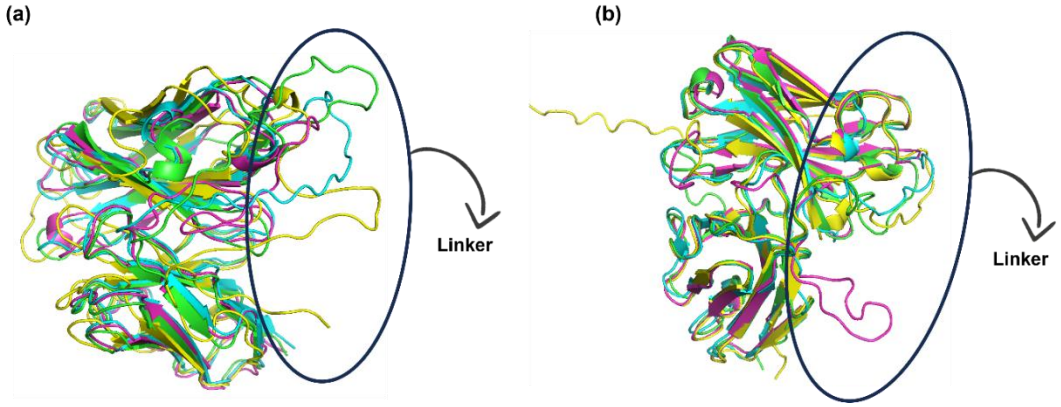


**Figure 0.1** Represents the superimposed structures of all the models generated. (A) anti-IL-6 scFv models obtained from i-TASSER (Pink), Phyre2 (Yellow), SwissModel (Green) and AlphaFold (Blue); (B) Anti-TNF-α scFv models obtained from i-TASSER (Green), Phyre2 (Pink), SwissModel (Blue) and AlphaFold (yellow). The linker is highlighted to illustrate structural differences

To evaluate the stereochemical quality of the predicted structures, the quality scores and Ramachandran plots were generated for each model using the SAVES server. ERRAT analyses the statistics of non-bonded interactions between different atoms and plots the values of the error vs position of 9-residue sliding window, calculated by comparing the statistics from extremely refined structures **(Elrashedy *et al.*, 2024)**. PROCHECK was used to evaluate the stereochemical quality of the protein model by analysing the residue-by-residue geometry and overall structure geometry. The Ramachandran plots assessed the distribution of phi (Φ) and psi (Ψ) dihedral angles, which categorize the amino acid residues in favoured, allowed and disallowed regions. This data reflects the structural reliability and conformation accuracy **(Ho & Brasseur, 2005; Hollingsworth & Karplus, 2010)**.

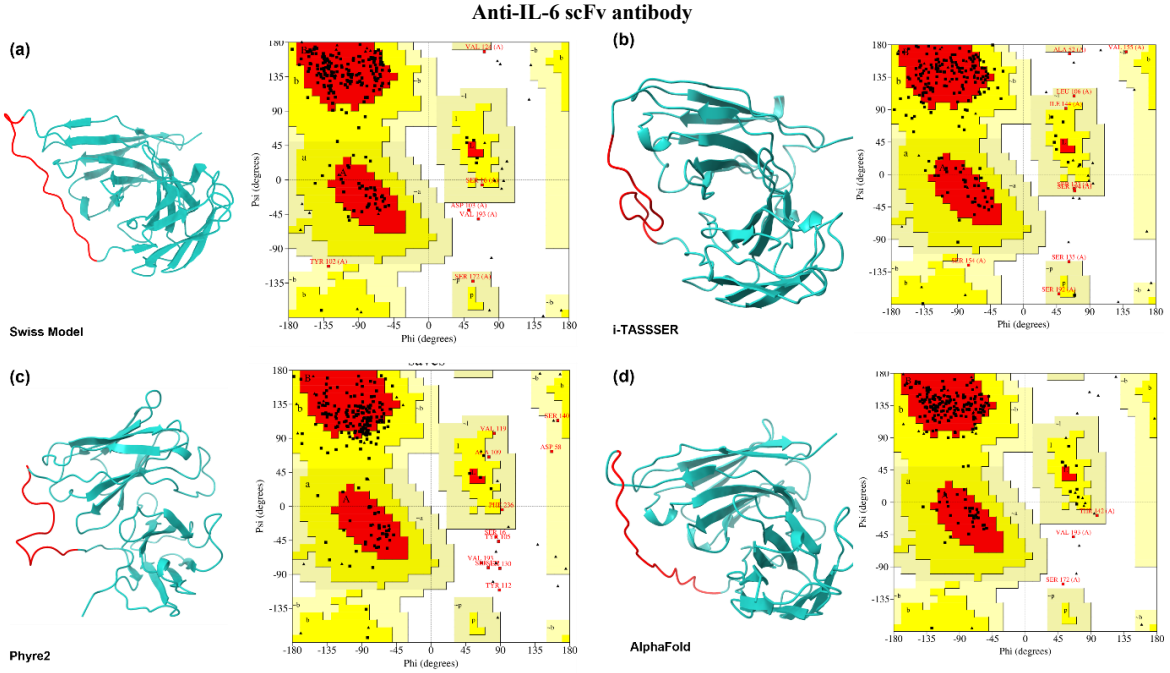


**Figure 0.2** Represents all the structures of murine anti-IL-6 scFv predicted by tools with their quality assessment using Ramachandran plots. All the structures consist of a heavy chain, light chain and a linker (red) joining the two chains. (A) Structure obtained from SwissModel; (B) Structure obtained from i-TASSER; (C) Structure obtained from Phyre2; and (D) Structure obtained from AlphaFold

**Table 2** ERRAT quality score and favoured region amino acid percentage of anti IL-6 scFv obtained from SAVES server

| S. No. | Server | ERRAT quality score | Favoured region | Allowed region |
|---|---|---|---|---|
| **1** | i-TASSER | 79.73 | 73.7 % | 22 % |
| **2** | Phyre2 | 48.68 | 73.5 % | 21.1 % |
| **3** | SwissModel | 93.13 | 86.3 % | 13.7 % |
| **4** | AlphaFold | 95.85 | 88.3 % | 11.7 % |

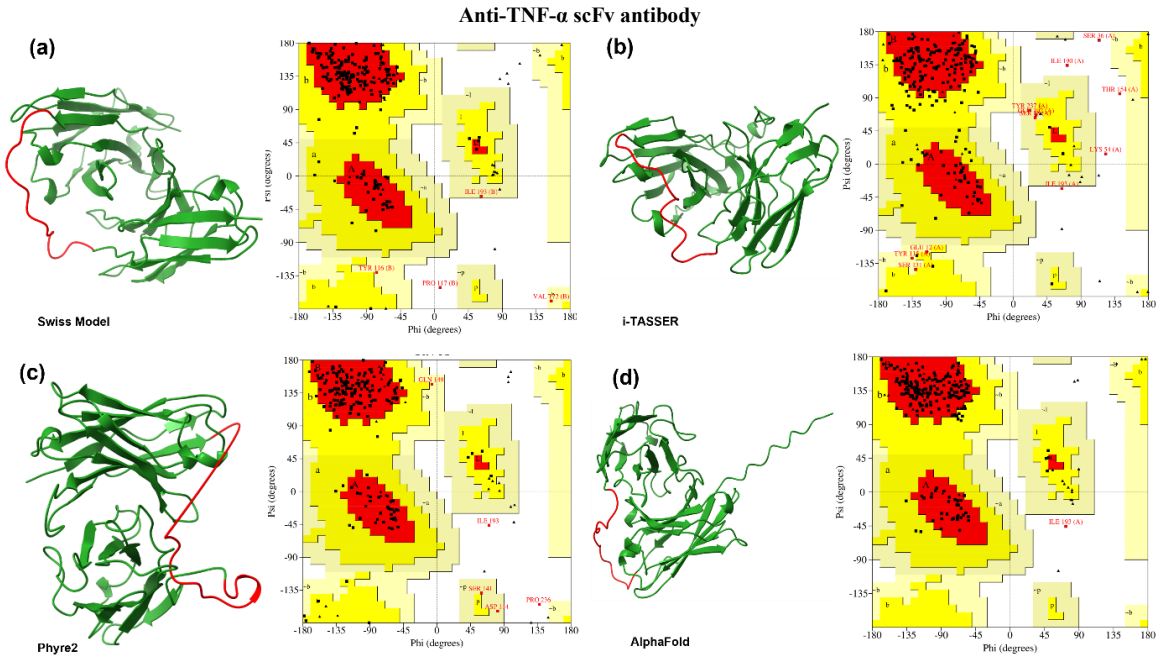


**Figure 0.3** Represents all the structures of murine anti-TNF-α scFv predicted by prediction tools with their quality assessment using Ramachandran plots. All the structures consist of a heavy chain, light chain and a linker (red) joining the two chains. (A) Structure obtained from SwissModel; (B) Structure obtained from i-TASSER; (C) Structure obtained from Phyre2; and (D) Structure obtained from AlphaFold

**Table 3** ERRAT quality score and favoured region amino acid percentage of anti-TNF-α scFv obtained from SAVES server

| S. No. | Server | ERRAT quality score | Favoured region | Allowed region |
|---|---|---|---|---|
| **1** | i-TASSER | 79.64 | 74.6 % | 20 % |
| **2** | Phyre2 | 43.65 | 86.5 % | 11.5 % |
| **3** | SwissModel | 92.72 | 90.2 % | 8.3 % |
| **4** | AlphaFold | 95.45 | 92.2 % | 7.3 % |

Based on the data presented in

***Table 2*** and

***Table 3***, the AlphaFold model achieved the highest quality score of 95.85% and 88.3% residues in favoured region in case of anti-IL-6 scFv, whereas, the score was 95.45% and 92.2% of residues in favourable region in case of anti-TNF-α scFv. SwissModel followed as the second best performed model after AlphaFold, with quality score of 93.13% with 86.3% residues in favourable region in case of anti-IL-6 scFv. The similar trend was observed in case of anti-TNF-α scFv with the ERRAT score of 92.72 and 90.2% residues in most favourable region, demonstrating higher reliability. Phyre2 and i-TASSER yielded low ERRAT scores with higher percentage of residues in allowed regions. This suggests a low optimal geometry and less reliability in flexible regions, such as linker region in the case of an scFv.
**Figure** 0.2 and **Figure** 0.3 shows the predicted structures and their Ramachandran plots, which visually confirm the superior quality of AlphaFold structure, followed by SwissModel structure. The AlphaFold shows the tight clustering of residues in favoured β-sheets and α-helical regions with minimal residues in disallowed regions. SwissModel demonstrated a relatively similar pattern.

**Selection of SwissModel for further analysis**

Although AlphaFold generates the highest quality structures, its use was prohibited for subsequent protein-protein docking and screening due to restrictions imposed by the AlphaFold server as stated in AlphaFold server output terms of use (AlphaFold Server, 2024). Consequently, the SwissModel structure was identified as the second-best structure after AlphaFold, as described in above sections. Due to this reason the SwissModel's structures were utilized for the protein-protein docking studies, followed by MD simulations.

**Identification of CDR sequences of CDR1, CDR2, and CDR3**

The identification of CDRs in the protein sequence was performed using a free online bioinformatics tool as mentioned in section 0. They were identified using various annotation methods, such as Kabat, IMGT, and Chothia numbering schemes. The IMGT scheme was employed in the present study. **Figure** 0.4 represents the CDRs in both the scFv, which are marked in distinctive colours. The results are summarised in

**Table *4*** and Table ***5*** for heavy and light chains, respectively.

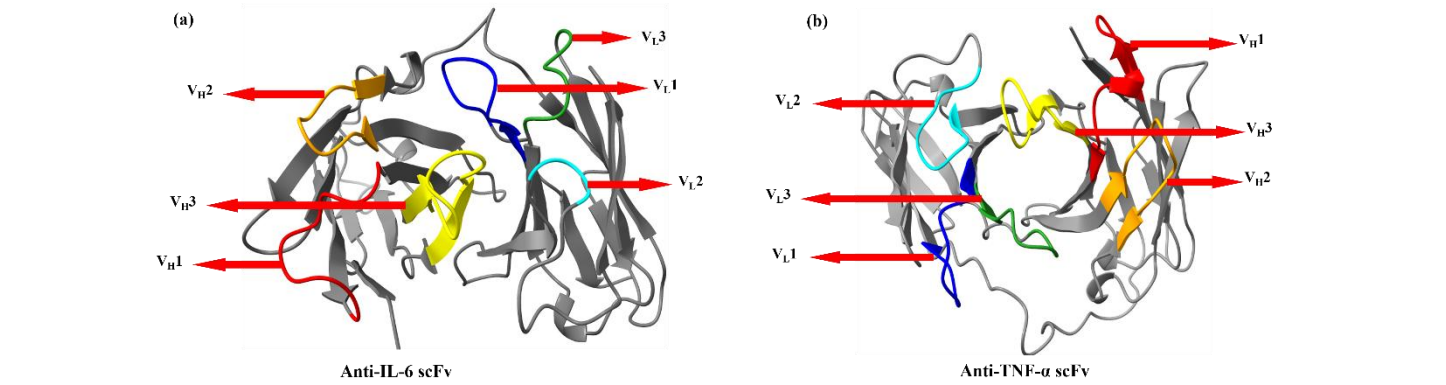


**Figure 0.4** The CDRs are illustrated for (A) Anti-IL-6 scFv and (B) Anti-TNF-α scFv in red (VH1), Orange (VH2), Yellow (VH3), Dark blue (VL1), cyan (VL2) and green (VL3)

**Table 4** Complementarity Determining Regions for heavy chain

| S. No. | CDRs | Anti-IL-6 scFv | A.A. range | Anti-TNF-α scFv | A.A. range |
|---|---|---|---|---|---|
| **1** | $V_H1$ | GFSLSTSGMG | 27 – 36 | KASGYSFTGYTMS | 34 – 47 |
| **2** | $V_H2$ | IWWDDDKY | 54 - 61 | LINPYNGGTS | 61 – 69 |
| **3** | $V_H3$ | ARSYDDYLYYALDY | 99 - 112 | ARGGYDDYYPMDY | 108 - 120 |

**Table 5** Complementarity Determining Regions for light chain

| S. No. | CDRs | Anti-IL-6 scFv | A.A. range | Anti-TNF-α scFv | A.A. range |
|---|---|---|---|---|---|
| **1** | $V_L1$ | QSISDY | 169 – 174 | SASSSVSYMY | 167 – 176 |
| **2** | $V_L2$ | SVS | 192 – 194 | IYEISKLA | 190 – 197 |
| **3** | $V_L3$ | QNGHSFPLT | 231 - 239 | CQQWNYPY | 240 - 247 |

The identification of CDRs demonstrates a thorough grasp of antibody binding regions. These identified CDRs provide a crucial basis for subsequent analyses, including protein-protein docking and molecular dynamic simulations, which are used to evaluate antigen binding interactions.

**Molecular docking**

The HADDOCKv2.4 application executed protein-protein docking simulations to analyse scFv antibody binding with its antigen target through protein-protein interaction assessment. The docking procedure was initiated using the scFv antibody structure produced by protein structure modelling technique as discussed in section 0. HADDOCK utilized earlier determined CDRs during docking by selecting active residues that prioritized antigen-binding site interactions. Multiple docking runs were executed to explore the binding modes across different combinations with respective scFv values. Lower the HADDOCK score, stronger is the binding **(Martarelli *et al.*, 2024a)**

**Anti-IL-6 scFv antibody**

HADDOCK generated a total of 10 clusters with top 4 best docked complexes in each cluster. The results are released in a way that the top cluster remains the most reliable according to the server. The data also shows the Z-score which indicates the standard deviation from the average, that particular cluster is located in terms of score. The top 5 cluster results for all the docking combinations are shown in tabular form below.

***Anti-IL-6 scFv with human IL-6***

When the murine anti-IL-6 scFv was docked with human IL-6 (PDB ID: 1ALU), the cluster 3 obtained the lowest HADDOCK score of 2.6 ± 3.3, which has RMSD of 14.1 ± 0.2 and the Z-score of – 2.4. This indicates that the cluster 3 is extremely favourable and structurally consistent binding. Table 6 shows the HADDOCK scores, cluster size, RMSD and Z-scores of the top 5 clusters. **Figure** 0.5 indicates the graphical representation of all the cluster data based on different energies, which are, van der Waals, electrostatic and restraints energy. All graphs demonstrated that the cluster 3 is the best of all.

**Table 6** Data shows the docking scores, RMSD and Z-scores of top 5 clusters obtained after docking of anti-IL-6 scFv with human IL-6.

| Cluster No. | HADDOCK score | Cluster size | RMSD | Z-score |
|---|---|---|---|---|
| **Cluster 3** | 2.6 ± 3.3 | 15 | 14.1 ± 0.2 | - 2.4 |
| **Cluster 10** | 27.4 ± 35 | 5 | 1.3 ± 0.8 | - 1.1 |
| **Cluster 2** | 41.2 ± 7.4 | 32 | 9.7 ± 0.3 | - 0.5 |
| **Cluster 5** | 53.1 ± 7.1 | 6 | 11.9 ± 0.1 | 0.1 |
| **Cluster 1** | 54.1 ± 5.2 | 33 | 17.1 ± 0.4 | 0.2 |

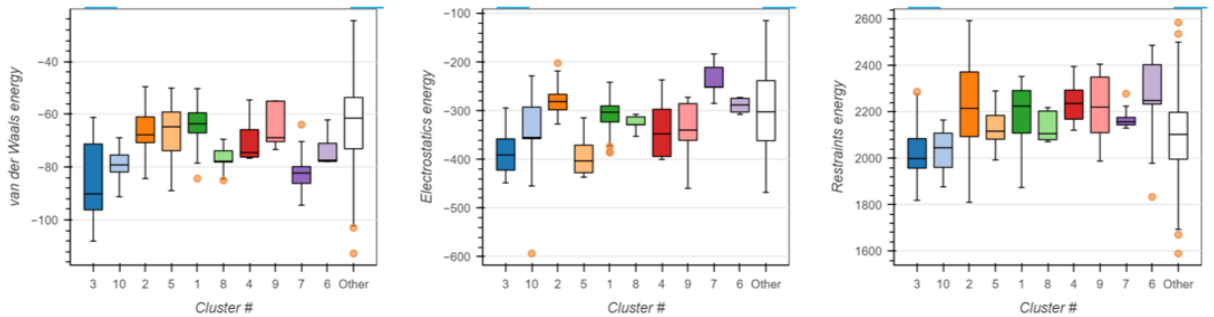


**Figure 0.5** Graphical representation of all the clusters after docking based on van der Waals energy, Electrostatic energy and Restraints energy anti-IL-6 scFv with human IL-6

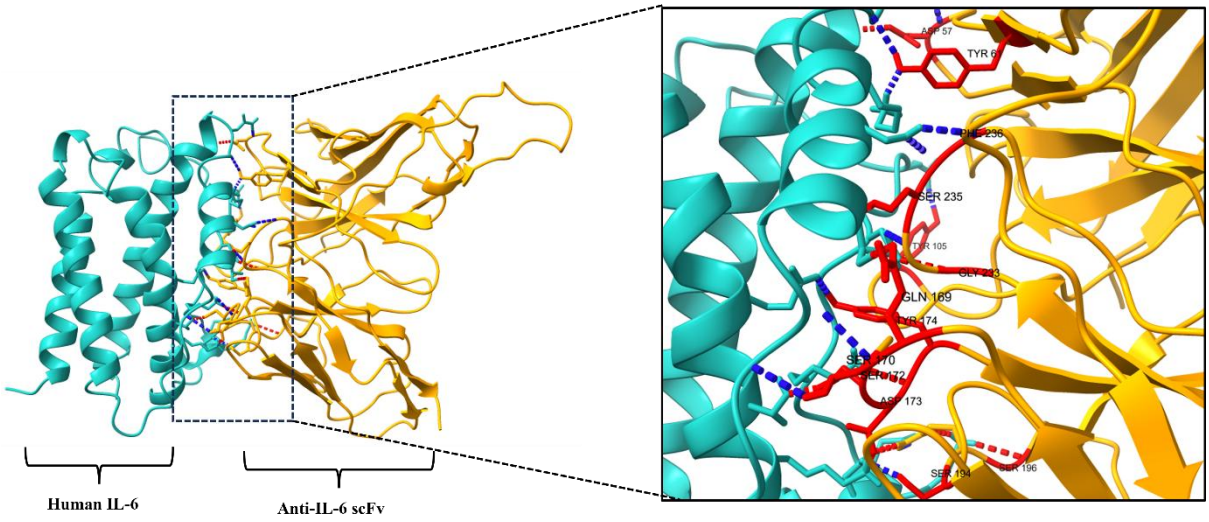


**Figure 0.6** Represents the interaction between anti-IL-6 scFv (Yellow) and human IL-6 (light sea green). Interacting CDRs are highlighted in red colour and labelled

The leading model of cluster 3 was analysed for the H-bonds interaction, which is illustrated in **Figure** 0.6 and detailed bonds and bond lengths are mentioned in Table 7. The CDRs of anti-IL-6 scFv interacted very efficiently with human IL-6, forming extensive H-bond networks critical for specificity and stability of the complex. The scFv and human IL-6 formed nearly 22 H-bonds in total with each other and out of which 18 bonds were made with the amino acids present in the CDR regions. This extensive H-bonds network with shorter bond length (1.6Å – 2.6Å) driven by all the CDRs suggests strong affinity and shows consistent binding with its primary target i.e. IL-6.

**Table 7** Shows the CDR hydrogen bonds formed between anti-IL-6 scFv (Chain B) and human IL-6 (Chain A)

| S. No. | H-bonds (donor) | H-bonds (acceptor) | Length of H-bond (Å) | CDR |
|---|---|---|---|---|
| **1** | /A ASN 64 | /B GLY 233 | 1.968 | ✔ |
| **2** | /A ASN 64 | /B HIS 234 | 2.638 | ✔ |
| **3** | /A LYS 67 | /B ASP 173 | 1.941 | ✔ |
| **4** | /A LYS 87 | /B ASP 173 | 1.61 | ✔ |
| **5** | /A ASP 141 | /B SER 170 | 2.355 | ✔ |
| **6** | /A THR 144 | /B GLN 169 | 1.736 | ✔ |
| **7** | /A SER 147 | /B PHE 236 | 2.134 | ✔ |
| **8** | /A LYS 151 | /B TYR 61 | 1.733 | ✔ |
| **9** | /A ASN 156 | /B ASP 57 | 2.518 | ✔ |
| **10** | /A LEU 159 | /B ASP 57 | 1.919 | ✔ |
| **11** | /B TYR 61 | /A ALA 154 | 2.309 | ✔ |
| **12** | /B TYR 105 | /A GLU 60 | 1.642 | ✔ |
| **13** | /B SER 170 | /A THR 139 | 2.374 | ✔ |
| **14** | /B SER 172 | /A THR 90 | 1.802 | ✔ |
| **15** | /B TYR 174 | /A GLU 94 | 1.7 | ✔ |
| **16** | /B SER 194 | /A ASP 72 | 2.552 | ✔ |
| **17** | /B SER 235 | /A THR 144 | 1.791 | ✔ |
| **18** | /B PHE 236 | /A SER 147 | 2.423 | ✔ |

***Anti-IL-6 scFv with human IL-11***

The docking of murine anti-IL-6 with human IL-11 (PDB ID: 6O4O) acts as a control where it was performed to assess the potential cross-reactivity. The best cluster of all was cluster 1 with the HADDOCK score of 19.0 ± 3.4. The RMSD was noted to be 0.4 ± 0.2 and the z-score was – 2.1 as shown in Table 8. The similar trend can also be observed in the graphical representation as presented in **Figure** 0.7.

**Table 8** Data shows the docking scores, RMSD and Z-scores of top 5 clusters obtained after docking of anti-IL-6 scFv with human IL-11

| Cluster No. | HADDOCK score | Cluster size | RMSD | Z-score |
|---|---|---|---|---|
| **Cluster 1** | 19.0 ± 3.4 | 28 | 0.4 ± 0.2 | - 2.1 |
| **Cluster 5** | 33.2 ± 5.7 | 11 | 5.1 ± 0.7 | - 1.2 |
| **Cluster 8** | 38.6 ± 13.9 | 6 | 11.1 ± 0.5 | - 0.9 |
| **Cluster 2** | 54.1 ± 14.2 | 14 | 15.5 ± 0.1 | 0.1 |
| **Cluster 9** | 59.3 ± 2.6 | 5 | 17.8 ± 0.1 | 0.4 |

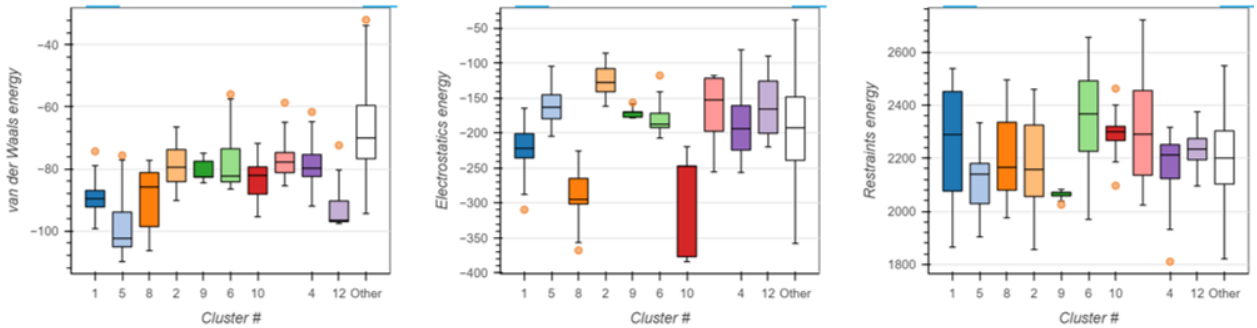


**Figure 0.7** Graphical representation of all the clusters after docking based on van der Waals energy, Electrostatic energy and Restraints energy for anti-IL-6 scFv with human IL-11

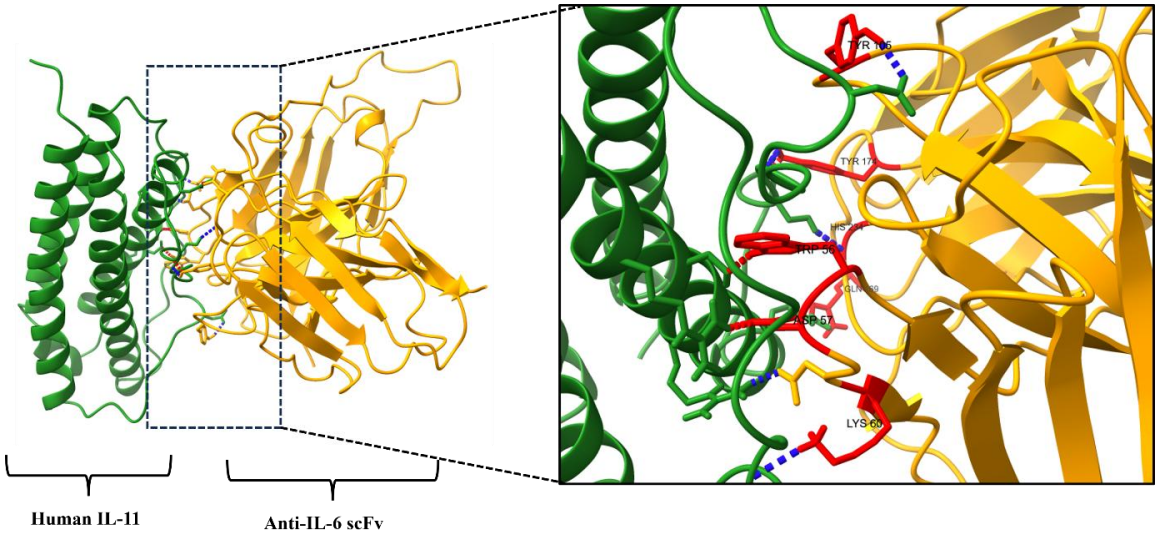


**Figure** 0.8 Represents the interaction between anti-L-6 scFv (Yellow) and human IL-11 (Green). Interacting CDRs are highlighted in red colour and labelled

The top model from cluster 1 was taken for the H-bond analysis utilizing ChimeraXv1.9 software. It can be clearly noted from **Figure** 0.8 and Table 9, the interaction between murine anti-IL-6 scFv and human IL-11 is barely favourable, when compared with human IL6. The reduced number of H-bonds with longer bond lengths (2.6Å – 3.2Å) and higher value of HADDOCK score in this case is a direct indication of weaker binding. This suggests the limited cross-reactivity with IL-11. The CDRs selected during the docking process engage effectively but the interaction is less optimal which is likely due to the structural differences in the IL-11 epitope.

**Table 9** Shows the CDR hydrogen bonds formed between anti-IL-6 scFv (Chain B) and human IL-11 (Chain A)

| S. No. | H-bond (Donor) | H-bond (acceptor) | Length of H-bond (Å) | CDR |
|---|---|---|---|---|
| **1** | /A SER 60 | /B HIS 234 | 2.940 | ✔ |
| **2** | /A ALA 61 | /B TYR 174 | 2.862 | ✔ |
| **3** | /A GLN 68 | /B GLN 169 | 3.084 | ✔ |
| **4** | /A ARG 77 | /B ASP 59 | 2.719 | ✔ |
| **5** | /A ARG 85 | /B ASP 57 | 2.703 | ✔ |
| **6** | /B TRP 56 | /A SER 82 | 2.730 | ✔ |
| **7** | /B LYS 60 | /A PRO 133 | 3.181 | ✔ |
| **8** | /B TYR 105 | /A ASP 52 | 3.217 | ✔ |
| **9** | /B TYR 174 | /A MET 59 | 2.607 | ✔ |

**Anti-TNF-α scFv**

***Anti-TNF-α scFv with human TNF-α***

The protein-protein docking of murine anti-TNF-α scFv with human TNF-α (PDB ID: 1TNF) gave cluster 1 as the best cluster with the HADDOCK score of 38.5 ± 6.3, RMSD of 13.3 ± 0.1 and the Z-score of -1.6 as shown in Table 10, which indicates the favourable and structurally convenient binding of the protein. The corresponding graphical representation is shown in **Figure 0.9** for the same.

**Table 10** Data shows the docking scores, RMSD and Z-scores of top 5 clusters obtained after docking of anti-TNF-α scFv with human TNF-α

| Cluster No. | HADDOCK score | Cluster size | RMSD | Z-score |
|---|---|---|---|---|
| **Cluster 1** | 38.5 ± 6.3 | 19 | 13.3 ± 0.1 | - 1.6 |
| **Cluster 5** | 47.0 ± 11.7 | 9 | 17.8 ± 0.5 | - 1.2 |
| **Cluster 3** | 49.8 ± 15.1 | 11 | 17.5 ± 0.1 | - 1.0 |
| **Cluster 4** | 62.2 ± 17.2 | 9 | 12.1 ± 0.0 | - 0.5 |
| **Cluster 9** | 67.2 ± 14.2 | 5 | 16.8 ± 0.5 | - 0.2 |

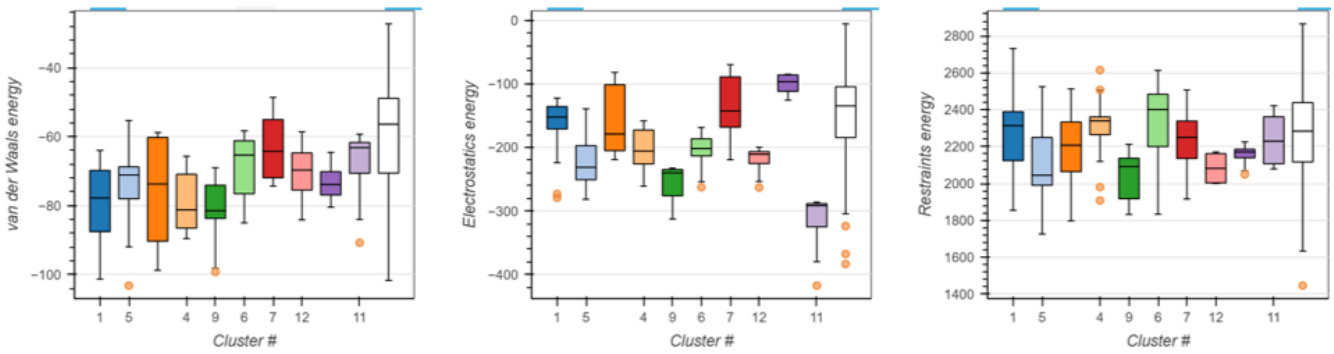


**Figure 0.9** Graphical representation of all the clusters after docking based on van der Waals energy, Electrostatic energy and Restraints energy for anti-TNF-α scFv and human TNF-α

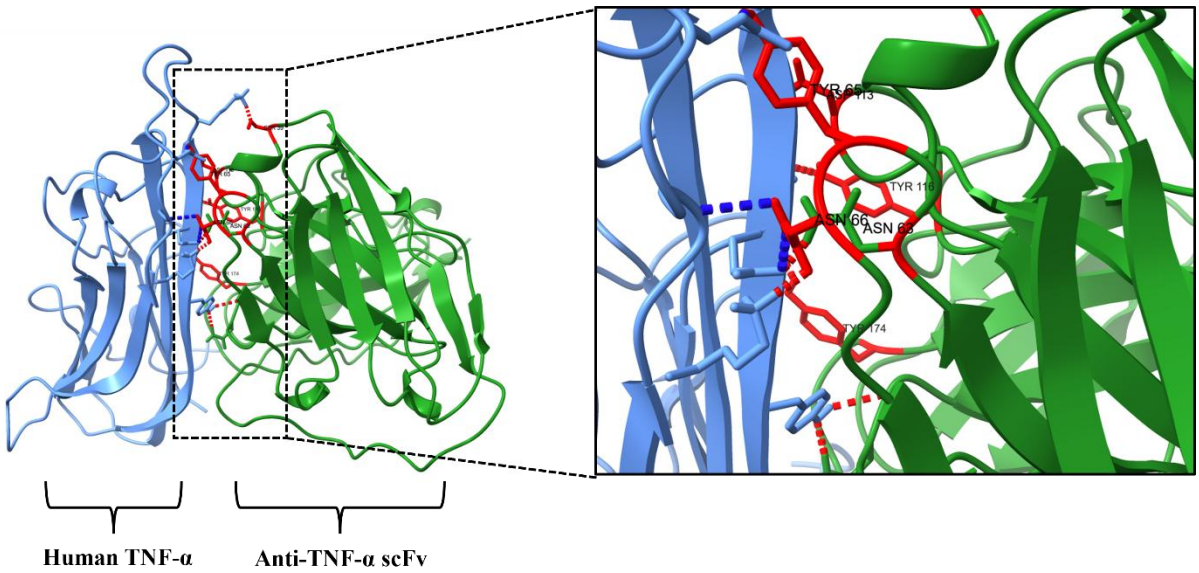


**Figure** 0.10 Represents the interaction between anti-TNF-α scFv (Green) and human TNF-α (Blue). Interacting CDRs are highlighted in red colour and labelled

The top model from the best cluster was carried forward for the H-bonds analysis where **Figure** 0.10 and Table 11 specifically represents the H-bonds which are formed between the two proteins with the amino acids interacting and the bond lengths. The data shows that out of total 11 H-bonds, 9 bonds were formed by the interaction of amino acids present in the CDR regions. The bond length of the formed shorter H-bonds which varies from 1.643Å to 2.852Å. This advocates that the proteins have high affinity towards each other and it strongly binds to its primary target, i.e. TNF-α.

**Table 11** Shows the CDR hydrogen bonds formed between anti-TNF-α scFv (Chain B) and human TNF-α (Chain A)

| S. No. | H-bond (Donor) | H-bond (Acceptor) | Length of H-bond (Å) | CDR |
|---|---|---|---|---|
| **1** | /A LYS 98 | /B ASN 66 | 1.664 | ✔ |
| **2** | /A LYS 112 | /B SER 39 | 1.85 | ✔ |
| **3** | /A SER 47 | /B TYR 116 | 2.06 | ✔ |
| **4** | /A GLN 149 | /B ASP 113 | 2.156 | ✔ |
| **5** | /B ASN 63 | /A GLU 116 | 1.705 | ✔ |
| **6** | /B TYR 65 | /A GLU 104 | 1.643 | ✔ |
| **7** | /B ASN 66 | /A PRO 100 | 2.852 | ✔ |
| **8** | /B ASN 66 | /A GLU 116 | 2.634 | ✔ |
| **9** | /B TYR 174 | /A GLY 148 | 1.894 | ✔ |

***Anti-TNF-α with TNF-β***

Protein-protein docking of murine anti-TNF-α scFv and human TNF-β (PDB ID: 1TNR) gave cluster 5 as the best cluster out of all with the HADDOCK score of 109.0 ± 22.9, RMSD of 0.9 ± 0.7 and the Z-score of -1.5. The information of top 5 best clusters is shown in Table 12 and Figure 0.11 with cluster names, their respective HADDOCK scores, cluster size, RMSD and Z-scores. Observing the data shows that the docked proteins are not structurally convenient as compared to the earlier docking of anti-TNF-α with human TNF-α which is the primary target and not TNF-β.

**Table 12** Data shows the docking scores, RMSD and Z-scores of top 5 clusters obtained after docking of anti-TNF-α scFv with human TNF-β

| Cluster No. | HADDOCK score | Cluster size | RMSD | Z-score |
|---|---|---|---|---|
| **Cluster 5** | 109.0 ± 22.9 | 5 | 0.9 ± 0.7 | - 1.5 |
| **Cluster 1** | 115.5 ± 2.1 | 12 | 16.0 ± 0.4 | - 1.3 |
| **Cluster 2** | 134.0 ± 5.2 | 11 | 21.6 ± 0.1 | - 0.9 |
| **Cluster 10** | 159.2 ± 13.5 | 4 | 17.9 ± 0.2 | - 0.4 |
| **Cluster 9** | 159.5 ± 24.5 | 4 | 7.3 ± 0.5 | - 0.4 |

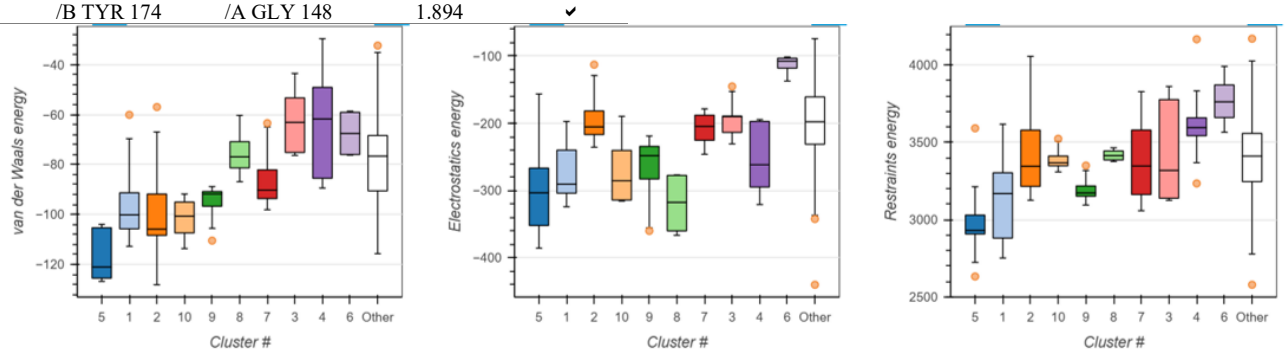


**Figure** 0.11 Graphical representation of all the clusters after docking based on van der Waals energy, Electrostatic energy and Restraints energy for anti-TNF-α scFv with human TNF-β

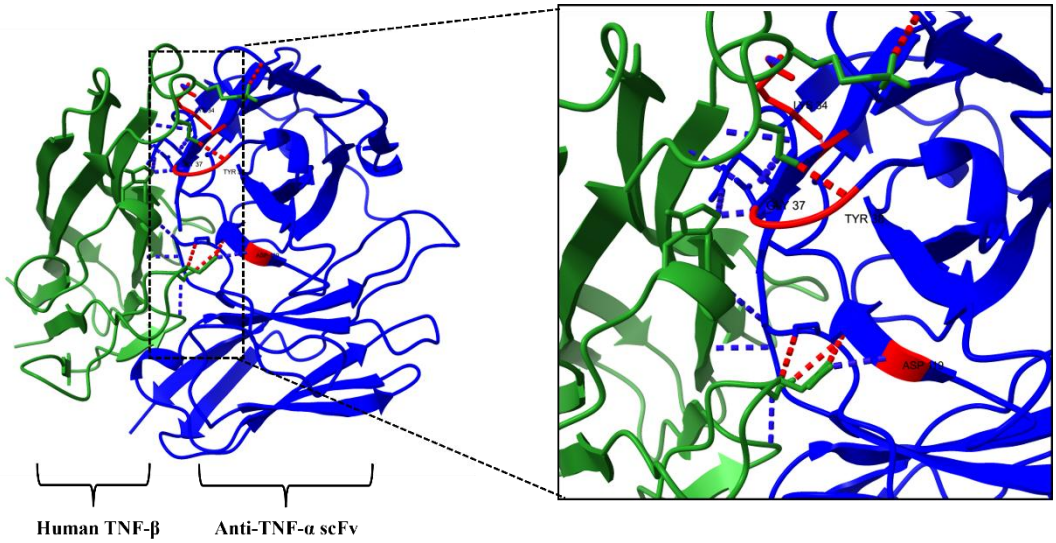


**Figure** 0.12 Represents the interaction between anti-TNF-α scFv (Blue) and human TNF-β (Green). Interacting CDRs are highlighted in red colour and residues are labelled

The top model of cluster 5 was taken for H-bond analysis with ChimeraX software. The comprehensive data of all the H-bonds formed is represented in **Figure** 0.12 and

Table ***13***, which shows the amino acids taking part in H-bond formation and the bond lengths. The table shows that total 14 bonds were formed and out of which only 4 bonds were made where amino acids from CDRs were engaged. The data also shows the longer bond length as compared to docking of anti-TNF-α scFv with human TNF-α. The bond length ranges from 2.621Å to 3.57Å.

**Table 13** Shows the CDR hydrogen bonds formed between anti-TNF-α scFv (Chain A) and human TNF-β (Chain B)

| S. No. | H-bond (Donor) | H-bond (Acceptor) | Length of H-bond (Å) | CDR |
|---|---|---|---|---|
| **1** | /A LYS 34 | /B LYS 89 | 2.671 | ✔ |
| **2** | /A GLY 37 | /B SER 87 | 2.951 | ✔ |
| **3** | /B ASN 41 | /A ASP 119 | 2.857 | ✔ |
| **4** | /B SER 87 | /A TYR 38 | 2.799 | ✔ |

The longer bond lengths and a lesser number of CDR amino acids interactions indicate the weaker binding. This reflects the specificity of scFv towards its primary target. The extended bond lengths suggest less optimal CDR-epitope complementarity which is likely due to subtle structural differences between TNF-α and TNF-β.

Binding interactions were experimentally validated using ELISA in a previous study **(Pourtaghi-Anvarian *et al.*, 2019)**, which demonstrated effective association between scFv and TNF-α. The present docking results were compared with these findings to assess consistency. Additionally, the obtained docking scores were evaluated in the context of other reported scFv–antigen systems, including scFv–EGFR and HuRABVscFv1–RABV-G complexes. Docking was performed using HADDOCK, and the resulting scores were found to be comparable with those reported in these studies **(Rezaei Adriani *et al.*, 2024)**.

**Molecular dynamic simulation**

The MD simulations were conducted to assess the stability, flexibility and dynamic behaviour of scFv and cytokines complexes derived from the docking models obtained previously. These models were subjected to 200ns MD simulation in solvent environment using GROMACS v2023.3. The simulations aimed to validate the docking predictions, evaluate the endurance of the H-bonds and observe the conformational changes over the time. Key metrics which were analysed were RMSD, RMSF, Rg, SASA and H-bonds.

**Root Mean Square Deviation (RMSD) analysis**

Stable RMSD values are widely used to measure structural stability and conformational convergence in MD simulations, where lower and more consistent RMSD values reflect a structurally compact, well-equilibrated system **(Kurniawan & Ishida, 2022)**. A smaller deviation in the RMSD indicates a more stable protein structure, and backbone RMSD calculated from Cα atoms is commonly employed to assess system-wide stability over the course of a simulation **(Aier *et al.*, 2016)**.

The RMSD analysis was performed with all the four complexes which are, anti-IL-6 scFv-human IL6 (aIL6scFv-hIL6), anti-IL-6 scFv-human IL11 (aIL6scFv-hIL11), anti-TNF-α scFv–human TNF-α (aTNFαscFv-hTNFα) and anti-TNF-α scFv–human TNF-β (aTNFαscFv-hTNFβ). RMSD was calculated for the protein backbones of both the scFv and the cytokine in each complex relative to their initial docked structures.

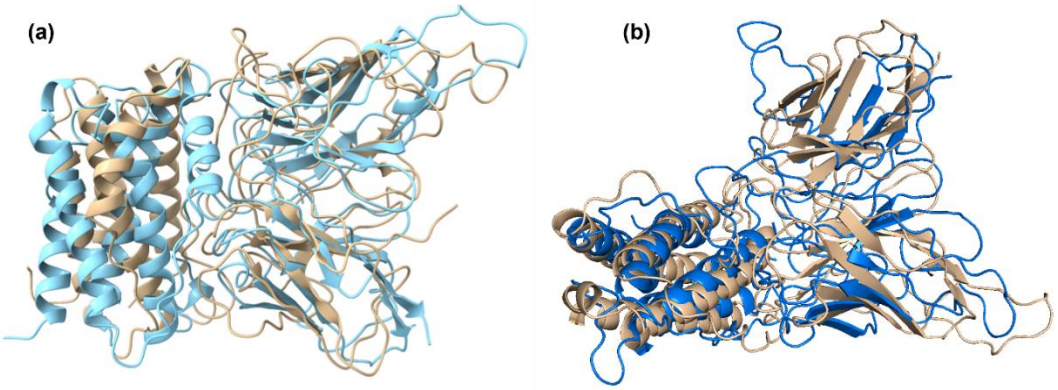


**Figure** 0.13 Superimposed structures of initial and final confirmations of (A) anti-IL-6 scFv – human IL-6 and (B) anti-IL-6 scFv – human IL-11. The RMSD of (A) is 4.303Å and (B) is 5.203Å

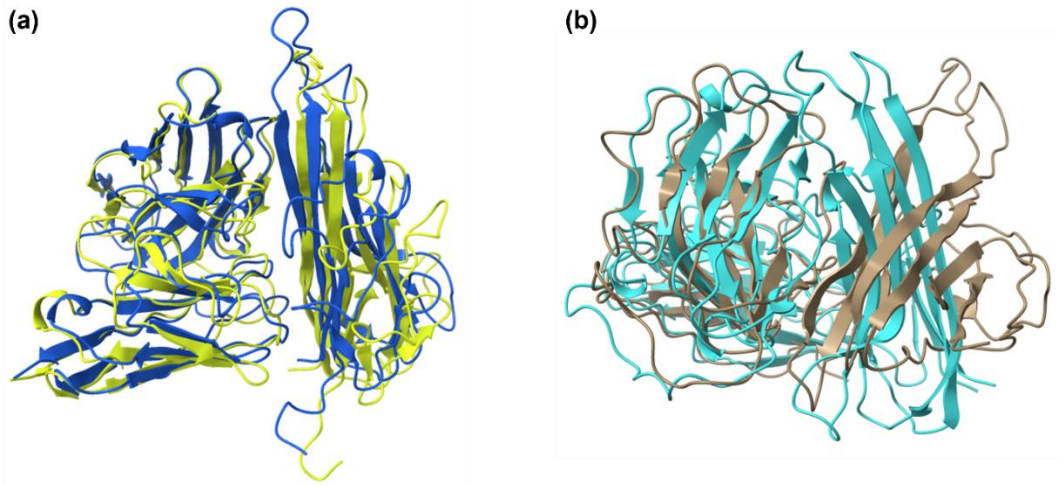


**Figure** 0.14 Superimposed structures of initial and final confirmations of (A) anti-TNF-α scFv – human TNF-α and (B) anti-TNF-α scFv – human TNF-β. The RMSD of (A) is 3.044Å and (B) is 3.233Å

Superimposed structures of the initial (t = 0ns) and final (t = 200ns) were analysed to visualise the conformational changes which is demonstrated in **Figure** 0.13 and **Figure** 0.14. RMSD time series graph was generated to access the stability dynamics over the simulation period as represented in **Figure** 0.15. The superimposition of initial and final structures has shown that the spatial shift of aIL6scFv-hIL6 is 4.303Å whereas, the spatial shift of aIL6scFv-hIL11 is 5.203Å. In case of aTNFαscFv-hTNFα, the spatial shift is 3.044Å and the shift is 3.233Å in case of aTNFαscFv-hTNFβ.

It was clearly observed that the spatial RMSD values were lower in case of interaction with the primary target, whereas, it was higher in case of control taken in form of another cytokine from same family. The lower spatial RMSD predicts that the interacting structures maybe stable and there might be a consistent bonding between the structures, reflecting the specificity of scFv molecule towards its primary target.

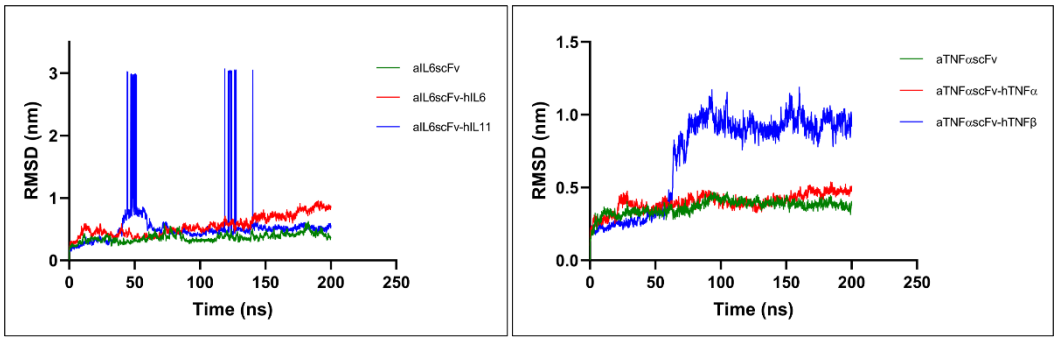


**Figure** 0.15 RMSD time series plots for (A) anti-IL-6 scFv and (B) anti-TNF-α scFv

The time series plot established in **Figure** 0.15 illustrates the frame-by-frame RMSD of the protein-protein complexes, where, the red plots denote the scFv interaction with its primary target, blue plot represents the interaction of scFv with another cytokine of same family (control) and green plots shows the frame-by-frame deviation of the un-bound scFv molecule.

The aIL6scFv system (green) demonstrates exceptional structural stability throughout the simulation period, maintaining the RMSD values consistently around 0.2nm to 0.3nm throughout the 200ns trajectory. This shows that the scFv protein adopts a stable conformation with minimal backbone fluctuations **(T. Wang & Duan, 2011)**.

In case of RMSD plot of aIL6scFv-hIL6, the RMSD values shows minor yet progressive increase in RMSD, plateauing at approximately 0.7–0.9 nm by the end of the trajectory. The slightly elevated RMSD compared to the unbound scFv suggests conformational adjustments upon IL-6 binding, which is typical for protein-protein interactions where induced-fit mechanisms contribute to complex formation and stabilization **(Okazaki *et al.*, 2023)**.

In contrast, the aIL6scFv–hIL11 complex (blue) exhibited pronounced conformational instability during the early-to-mid simulation period, characterized by sharp transient spikes reaching up to ~3.0 nm at approximately 45–50 ns and again between 125–140 ns. In antibody–antigen MD simulations, elevated RMSD fluctuations and failure to converge to an equilibrium state are strong indicators of structural instability at the binding interface, often reflecting a tendency toward ongoing or unresolved conformational changes **(Martarelli *et al.*, 2024b)**. These abrupt deviations are likely attributable to large-scale domain reorientations or transient dissociation events at the interface, reflecting the structural incompatibility between the anti-IL6 antibody and the non-cognate hIL11 ligand. Notably, after ~150 ns, the system appeared to re-equilibrate and settle to RMSD values comparable to the aIL6scFv–hIL6 complex; however, the overall trajectory suggests a less stable and more dynamically frustrated binding mode **(Schreiner *et al.*, 2012)**.

In the TNFα antibody system, a broadly similar but more moderate pattern was observed. The unbound aTNFαscFv (green) exhibits remarkable structural stability throughout the simulation time period, maintaining the RMSD values consistently between 0.3-0.4nm. In case of RMSD plot of aTNFαscFv-hTNFα, the RMSD values ranges from 0.4-0.5nm after ~75ns. The moderate fluctuations observed are characteristic of a stable protein-protein complex undergoing normal conformational motions. The overall RMSD is low which indicates structural adaptation upon binding while maintain overall complex integrity. In case of RMSD plot of aTNFα-hTNFβ (blue), the plot reveals markedly distinct behaviour. The system initially maintains stability comparable to other complex, but then undergoes a dramatic conformational transition between 50 to 75ns, with RMSD values rapidly increasing to approximately 0.9-1.1nm and remain elevated. Molecular recognition between an antibody and its antigen is not a static event but a dynamic process that hinges on the structural adaptability of both partners; when this complementarity is absent, the system fails to settle into a stable, low energy bound state **(Z. Wang *et al.*, 2025)**. This sustained high RMSD is indicative of structural instability at the antibody–antigen interface, likely arising from the structural divergence between hTNFα and hTNFβ.

**Radius of Gyration (Rg) analysis**

To complement the RMSD analysis and obtain a more complete picture of the structural dynamics of the simulated systems, the radius of gyration (Rg) was computed as a function of simulation time for all six systems. The compactness of the protein-protein complex was analysed using the Rg plot. This data provides the RMSD of particular atoms of the complex along its axis. The higher value of Rg infers that the protein is less compact and more flexible whereas the lower Rg value indicated that the protein is more compact and rigid **(Choudhury *et al.*, 2021)**. The Rg plots for anti-IL-6 scFv and anti-TNF-α scFv are displayed in **Figure** 0.16.

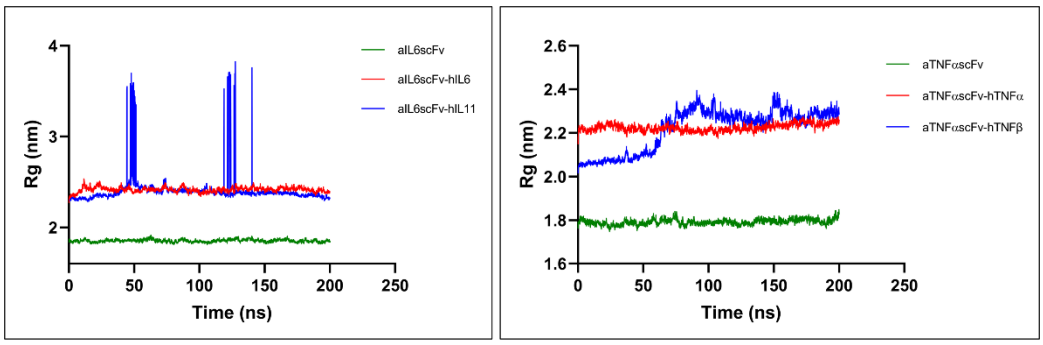


**Figure** 0.16 Radius of gyration (Rg) time series plot for (A) anti-IL-6 scFv and (B) anti-TNF-a scFv

The unbound aIL6scFv and aTNFαscFv display a consistently low Rg value, averaging around 1.9nm and 1.8nm throughout the simulation. This indicates that the scFv maintains its structural integrity in the absence of antigen, with minimal fluctuations.

The Rg increased marginally to an average of 2.4-2.5nm in case of aIL6scFv-hIL6 (red) This slight increase reflects the expected expansion due to antigen binding, yet the Rg remains stable over the trajectory of 200ns. The stable Rg indicates that the complex maintains a compact structure till the end of the simulation. This modest elevation in Rg, coupled with minimal fluctuations, is consistent with the formation of a compact and well-defined antibody-antigen complex. In case of aIL6scFv-hIL11 (Blue), the complex exhibits an Rg similar to that of the hIL6 complex. However, there was transient increase in Rg observed between 45-60ns and then again at around 125 to 140ns, with the values spiking up to ~3.8nm. This abrupt expansion is followed by a return to baseline levels, suggesting a significant, but temporary loss of compactness, potentially due to complex dissociation. These sharp excursions in Rg closely mirror the RMSD spikes observed in the same system and are strongly indicative of large-scale spatial expansion and loss of compact domain at the antibody-antigen interface. Such instability is indicative of weak or non-specific interactions between aIL6scFv and hIL11.

In case of aTNFαscFv-hTNFα (red) and aTNFα-hTNFβ complexes, exhibits higher Rg values, averaging around 2.1-2.2nm for most of the simulation. This increase in the Rg compared to the unbound scFv reflects the larger size of the complex due to the binding of hTNFα and hTNFβ, respectively. The scFv and hTNFα complex show less variability in Rg than the other complex, suggesting that the complex designed is thermodynamically favourable and structurally well-ordered bound state that persisted throughout the simulation timescale.

However, aTNFαscFv-hTNFβ complex shows particularly changed behaviour. Beginning around 50–75 ns, the Rg gradually increased from approximately 2.1 nm to ~2.3–2.4 nm, where it persisted raised and highly variable for the rest of the simulation. This sustained elevation in Rg, combined with persistent fluctuations, reflects a gradual and irreversible expansion of the complex, pointing toward ongoing conformational instability and possible loosening of interfacial contacts. This occurs possibly due to dynamic interactions between scFv and its binding partners. These findings provide valuable insights into the structural adaptability of aTNFαscFv upon binding to its targets and contribute to understanding its interaction stability under the present computational conditions.

Taken together, the Rg analysis provides strong supporting evidence for the conclusions drawn from the RMSD analysis. Both scFv antibodies adopt compact, well-ordered configurations in their free states and in complex with their primary targets, while engagement with non-primary targets leads to measurable and sustained increases in Rg. This reflects structurally expanded and dynamically unstable complexes. In computational evaluations of scFv antibody-antigen complexes, the Rg has been monitored alongside RMSD to predict dynamic behaviour and assess structural integrity, with stable, low Rg profiles supporting robust antigen-binding interactions **(Ghani *et al.*, 2023)**.

**Hydrogen bonds analysis**

To further interrogate the molecular basis of binding stability in both antibody systems, the number of intermolecular hydrogen bonds (H-bonds) formed at the antibody-antigen interface was monitored as a function of simulation time. The H-bonds play a very vital role in the stability of the protein. This analysis was performed to analyse the stability and breaking and forming of H-bonds by change in the amino acid and protein shape over the simulation time **(Bhale & Venkataraman, 2023)**. The higher number of H-bonds indicates more stability and lesser number of H-bonds infers lesser stability.

Antibody specificity is administered by the CDRs and antigen recognition is driven by multiple non-covalent forces, H-bonds being among the most defining, whose number and stability directly reflect the strength and selectivity of the interaction **(Yoshida *et al.*, 2019)**.

The MD simulation was performed to evaluate the stability and dynamics of the H-bonds between the complexes. The number of intermolecular H-bonds was calculated over the period of 200ns to assess the strength and persistence of the interaction networks. H-bonds time series plot is represented in **Figure** 0.17 providing insights about the stability of the complexes.

In the IL-6 antibody system (A), the aIL6scFv-hIL6 complex (red) exhibited a consistently higher and more constant number of interfacial H- bonds throughout the 200 ns trajectory. Following an initial period of rapid equilibration during which the H-bond count fluctuated between ~8–14, the system settled into a stable regime with an average of nearly 5–7 H-bonds maintained at any given point in time, with occasional peaks reaching up to 10–11 bonds. This sustained H-bonding pattern is typical of a well-established and persistent binding interface. In antibody-antigen complexes, the properties of hydrogen bonds, particularly their number and energetic contribution have been known to be amongst the most significant features for differentiating productive binding interactions from poorly docked or nonspecific ones **(Richard & Pantazes, 2025)**.

In contrast, the aIL6scFv-hIL11 complex (blue) displayed markedly more erratic hydrogen bond behaviour throughout the simulation. While the system initiated with a comparable number of H-bonds (~8–10), the trajectory was scattered by frequent and deep drops at multiple time points. The H-bond count fell to near zero, indicating almost complete disruption of the interfacial contact. These transient collapses in hydrogen bonding are consistent with the large RMSD spikes and Rg excursions observed in the same system, and jointly reflect intermittent detachment of the antibody-antigen interface. Loss of the native binding mode during MD simulation is primarily driven by the disruption of crucial hydrogen bond interactions at the interface. Complexes with lower binding affinity show higher degrees of such H-bond disruption, whereas high affinity complexes incline to conserve their interfacial hydrogen bond network throughout the trajectory.

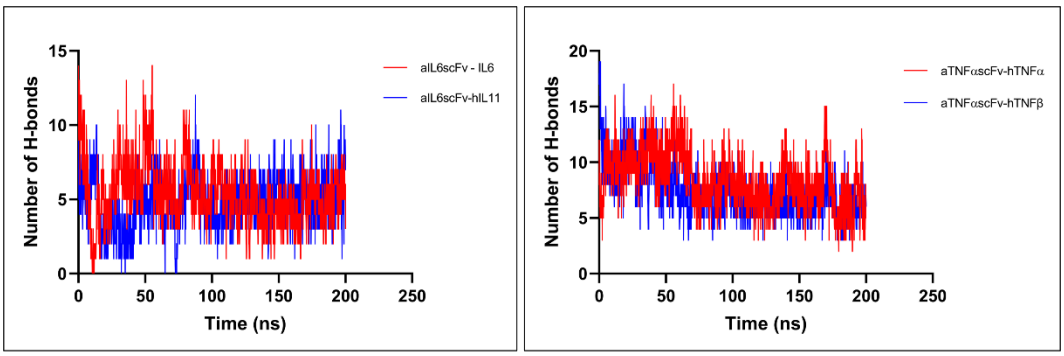


**Figure** 0.17 Number of intermolecular H-bonds time series plot for (A) anti-IL-6 scFv and (B) anti-TNFα scFv

In the TNFα antibody system (B), both complexes initiated with higher total numbers of interfacial hydrogen bonds, the aTNFαscFv-hTNFα (red) and aTNFαscFv-hTNFβ (blue) systems both exhibited H-bond counts of ~15–19 in the earliest frames. The aTNFαscFv-hTNFα complex (red) maintained a relatively higher and more uniform H-bond profile, averaging around 8–10 bonds with moderate fluctuations, but rarely dropping below 4–55 which is an indicative of a stable binding interface that was maintained throughout the simulation. The aTNFαscFv-hTNFβ complex (blue), while exhibiting a similarly high initial H-bond count, displayed considerably greater fluctuation and more frequent drops to lower H-bond numbers over the time. The trajectory was characterized by recurrent transient minima and high variance in H-bond counts, reflecting the inability of the antibody-antigen interface to combine into a stable H-bond network. Solvents play an important role in protein-protein interactions, and in antibody-antigen interactions. H-bonds mediate binding stability and specificity of recognition. Disruption of this H- bond network weakens and destabilizes the complex. Furthermore, greater affinity and specificity in antibody-antigen recognition are accomplished through the optimization of electrostatic and hydrogen bonding interactions at the binding site.

Taken together, the interfacial hydrogen bond analysis provides compelling molecular level predictions that both scFv antibodies form productive, stable, and persistent non-covalent interaction networks exclusively with their primary targets, while interactions with non-primary targets are characterized by erratic, intermittent, and significantly reduced hydrogen bonding.

**Solvent Accessible Surface Area (SASA) analysis**

To further illustrate the structural dynamics and solvent exposure behaviour of the antibody-antigen systems under study, the SASA was calculated as a function of simulation time for all systems. SASA is a quantity of particular interest in protein folding and functional studies, as it plays an important role in understanding the structure function relationship of proteins and is commonly used in computational studies to evaluate how protein surface regions interact with the aqueous environment **(Keskin, 2007)**.

SASA was calculated for the entire complex (i.e. scFv-cytokine) and for the individual scFv molecule. The time graphs are generated to assess the changes in solvent exposure over the simulation time period, providing insights in compactness, stability and conformational dynamics of the complexes. The protein's folding and unfolding can be observed by looking at the SASA plots as represented in Figure *0.18*.

The unbound aIL6scFv and aTNFαscFv exhibits a relatively stable SASA, fluctuating between approximately 130 and 150nm$^2$. This consistency suggests that the scFv maintains compact structure with limited exposure to the solvent, indicating structural stability in the absence of any antigen. The burial of hydrophobic residues is a key factor in protein folding, and the exposure of these residues to the solvent and the hydrophobic core is directly related to the stability of the protein.

In contrast, the aIL6scFv-hIL6 (red) show significantly higher SASA upon binding with hIL6 and hIL11. The hIL6 complex display notable fluctuations around 215-230nm$^2$. These fluctuations reflect the dynamic conformational adjustments at the protein-protein interfaces as the complex tries to stabilize. The aIL6scFv-hIL11 complex (blue) initially displayed a SASA comparable to the hIL6 complex (~200–215 nm²), but the trajectory was notably characterized by larger fluctuations and adjustment particularly in the 0–150ns window, before partially stabilizing in the later stages of the trajectory. It has been demonstrated that the bound conformation of biomolecules exhibits a higher SASA value compared to their unbound state, and instability in the SASA profile of a complex is suggestive of an inability to maintain stable interfacial contacts.

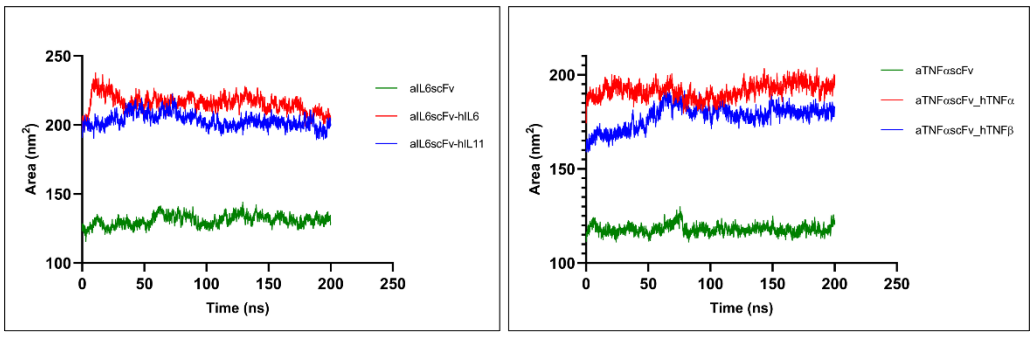


**Figure 0.18** Solvent Accessible Surface Area (SASA) time graphs for (A) anti-IL-6 scFv and (B) anti-TNF-α scFv

In relation to image (B), both scFv bound complexes displayed considerably higher SASA values (~175–200 nm²), as expected. However, the two complexes diverged in their respective SASA dynamics. The aTNFαscFv-hTNFα complex (red) maintained the highest and most stable SASA throughout the simulation, with values steadily near ~185–200 nm² and relatively modest fluctuations. This stable, SASA is indicative of a well sustained and consistently solvent exposed complex surface, reflecting a tightly bound and structurally coherent binding mode **(Liu *et al.*, 2024)**.

The aTNFαscFv-hTNFβ complex (blue), while initiating at comparable SASA values (~165–180 nm²) in the earlier simulation frames, displayed noticeably greater fluctuations throughout the trajectory and did not stabilize as cleanly as the hTNFα complex. The recurring variability in SASA with recurring fluctuations between higher and lower values is suggestive of conformational breathing at the binding interface, wherein the two molecular surfaces intermittently disengage and partially expose buried residues to solvent. Binding induced conformational transitions are linked with significant changes in solvent accessibility in the binding partners. The failure of the aTNFαscFv-hTNFβ system to converge to a well-defined SASA plateau is therefore a molecular level prediction of its reduced binding specificity and weakened interfacial stability.

Collectively, the SASA analysis reveals a consistent and coherent picture across both antibody systems: the free antibody fragments adopt compact, low SASA conformations. Primary target complexes form stable, well-maintained and elevated SASA profiles, while non-primary complexes are characterized by greater variance and fluctuations suggesting interfacial instability and inadequate complementarity between the antibody and its non-target cytokine.

**Root Mean Square Fluctuation (RMSF) analysis**

To gain residue-level insight into the local flexibility and dynamic behaviour of the antibody and antigen chains across the simulated systems, the RMSF of the Cα

atoms was calculated for each residue over the course of the 200ns MD trajectories. The RMSF measures the average deviation of a protein residue from a reference position. Regions with high RMSF values are typically more flexible, while regions with low RMSF values are typically more rigid **(AlAjmi *et al.*, 2021)**. The RMSF plots for aIL6scFv and aTNFαscFv are illustrated in Figure 0.19 and Figure 0.20, respectively.

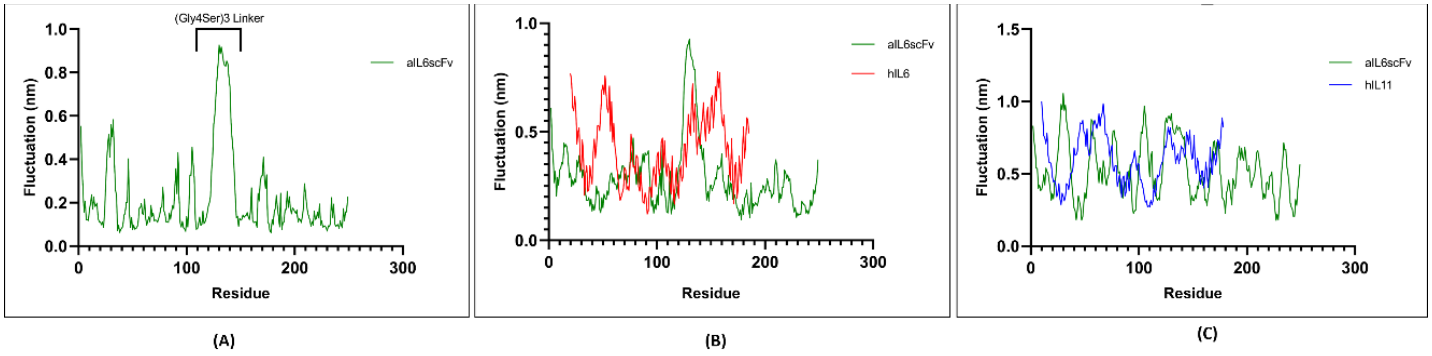


**Figure** 0.19 RMSF time series plot for (A) aIL6scFv, (B) aIL6scFv_IL6 and (C) aIL6scFv_IL11

The unbound aIL6scFv (A) showed fluctuations ranging from 0.1nm to 0.6nm. Most residues exhibited lower fluctuations of 0.1nm to 0.4nm, with peak at residue around 120, reaching 0.8nm. The lower fluctuations in most regions indicate the stability of the scFv's β-sheet framework, typically the VH and VL regions. The peak fluctuation of 0.6nm at residues from 126 to residues number 141 was shown by the linker region which connects the heavy and light chains in scFv molecule. This linker region mainly consists of amino acids such as glycine and serine. This reflects the inherent flexibility of the region which is consistent with the dynamic nature.

In aIL6scFv-hIL6 (B) complex, the RMSF ranges from 0.1nm to 0.9nm for aIL6scFv (green) and 0.1nm to 0.6nm in case of hIL6 (red). The peaks likely correspond to regions at protein-protein interaction interface. The reduced fluctuations in scFv and hIL6 upon binding with each other suggests a stable interaction primarily due to H-bonds present at the interface. The most flexible residues in case of scFv are present in the linker region which is a chain of glycine and serine. In case of hIL6, the most flexible residues are Met50, Cyc51, Glu52, Ser53, Ser54 and Lys55. The lower fluctuations in hIL6 at the core regions indicate the stability of its helical structure. The overall stability of the complex aligns with the low RMSD, stable Rg, high H-bonds counts and consistent SASA.

The aIL6scFv-hIL11 (C) complex presented a markedly different and more disordered flexibility landscape. The hIL11 antigen (blue) displayed persistently high and uniformly distributed RMSF values commonly between 0.5–1.0 nm across nearly its entire sequence. This elevated, broad fluctuation profile stands in sharp contrast to what might be expected of an antigen engaged in a stable, specific interaction, and is instead indicative of a largely unrestrained antigen that has failed to establish a stabilizing intermolecular contact network with the antibody. The most fluctuating regions are Gly10, Ser11, Phe43, Pro44, Asp46, Leu67, Ser144, Ser145, Ala146 and Trp147. It can be clearly noted from the plots, that the fluctuations are very high in this complex, as compared to aIL6scFv-hIL6 complex, which indicated that the binding is not stable as effectively, reflecting weaker interactions.

The RMSF analysis of the IL-6 antibody system reveals three mechanistically different behaviours: the free aIL6scFv displays characteristic CDR loop flexibility punctuated by the high amplitude motion of the (Gly$_4$Ser)3 linker; the primary complex shows moderate, interface localized fluctuations consistent with binding encouraged stabilization; and the non-primary complex is characterized by persistently high flexibility in both partners, reflecting the absence of specific and productive interfacial restraints.

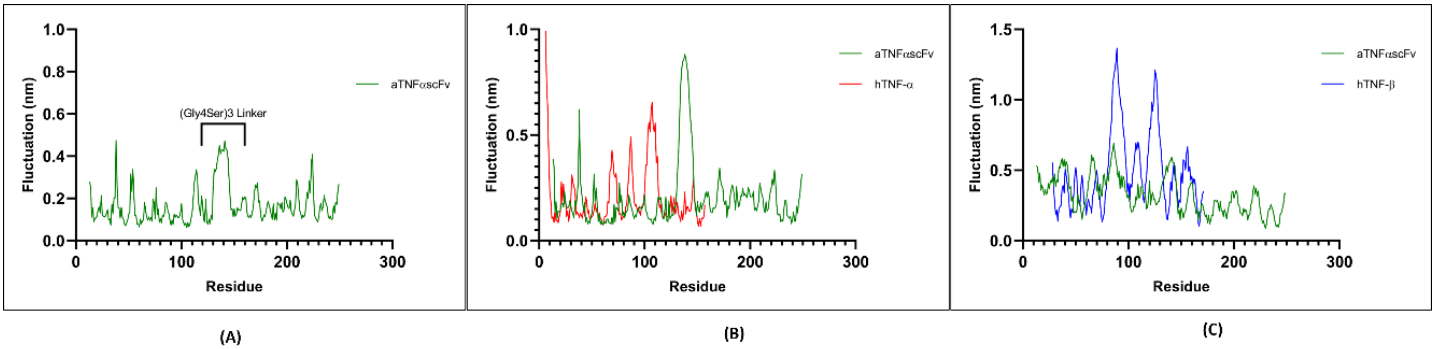


**Figure** 0.20 RMSF time series plot for (A) aTNFαscFv, (B) aTNFαscFv_TNFα and (C) aTNFα_TNFβ

The individual aTNFαscFv (A) shows the fluctuations in the range of 0.1nm to maximum of 0.5nm which is almost same as aIL6scFv, where the linker region shows the maximum fluctuation as shown in the figure. A particularly noteworthy feature of the free aTNFαscFv profile is the behavior of the (Gly$_4$Ser)3 linker region, annotated between approximately residues 130–165. The lower RMSF in both heavy and light chains infer that the scFv is very stable.

In case of aTNFαscFv-hTNFα (B) complex, the RMSF ranges from 0.1nm to 0.7nm in both aTNFαscFv and hTNFα. The major residues which show maximum fluctuations in case of hTNFα are Arg6, Thr7, Pro8, Cys69, Ser86, Tyr87, Arg103, Pro106, Glu107, Gly108, Ala109, and Glu110. The reduced fluctuations in scFv and the bound cytokine suggests the stabilization of these regions which is likely due to the H-bonds interaction at the interface. Few high peaks were observed during the course of simulation which likely to correspond to residues at the protein-protein interface or in the flexible loops that experience dynamic movements. The overall stability of the complex, well aligns with the low RMSD, stable Rg, high H-bonds, and coherent SASA plot. Crucially, the VH and VL framework residues and CDR loops outside the linker region showed well-controlled fluctuations, consistent with the stable and specific binding interaction supported by the RMSD, Rg, and hydrogen bond analyses for this system.

Whereas, in case of aTNFαscFv_TNFβ (C), the RMSD fluctuates between 0.2nm to 0.6nm for aTNFαscFv (green) and 0.2nm to the maximum of 1.4nm for hTNFβ (blue). The maximum fluctuations are observed in residues Lys28, Gln40, Ser70, Phe81, Lys84, Ala85, Tyr86, Ser87, Pro88, Lys89, Ala90, Thr91, Ser92, Ser93, Pro94, Leu95, Tyr96, Leu97, Ser106, Gln107, Tyr108, Pro109, Phe110, His111, Gln118, Lys119, Met120, Val121, Tyr122, Pro123, Gly124, Leu125, Gln126, Glu127, Pro128, Trp129, Leu130, and His131. The increased fluctuations in scFv regions of aTNFαscFv-hTNFβ as compared to aTNFαscFv-hTNFα indicates that the binding is not stable, reflecting weaker interaction interface. This complex shows significantly higher fluctuations and this increased dynamic is consistent with the lower number of H-bonds. This infers a less stable complex with partial dissociation.

The RMSF plots revealed distinct flexibility profiles for all the complexes. It was clearly noted that the complex with scFv binding to its primary target showed much lesser fluctuations indicating greater stabilization upon binding. The non-primary targets showed much higher fluctuations contributing to the reduced stability of the complex.

**Binding energy analysis**

MM-PBSA calculations were performed to estimate the absolute binding free energies ($\Delta G_{Total}$) for both the fully bound (complex) and completely unbound states of all scFv-cytokine complexes under investigation. The resulting binding free energy profiles produced values that verified the specificity and selectivity of each scFv construct toward its respective primary target cytokine. For the aIL-6

scFv system, the calculated $\Delta G_{Total}$ for the aIL6scFv-hIL6 complex (primary target) was determined to be -27.63 kcal/mol, whereas the corresponding value for the aIL6scFv-hIL11 complex (non-primary/cross-reactive target) was comparatively less favourable at -18.94 kcal/mol. Similarly, in the case of the anti-TNFα scFv construct, the $\Delta G_{Total}$ for the aTNFαscFv-hTNFα complex (primary target) was computed to be -36.24 kcal/mol, while the aTNFαscFv-hTNFβ complex (non-primary target) exhibited a marginally attenuated binding free energy of -33.95 kcal/mol. Collectively, a consistent and statistically coherent trend was observed across both scFv systems, where each scFv construct demonstrated markedly more negative $\Delta G_{Total}$ values which is indicative of thermodynamically more favourable and stable binding interactions with its primary target cytokine, relative to the non-primary cytokine target as represented in Figure 0.21. These findings interestingly suggest that both scFv constructs possess a pronounced thermodynamic preference and binding selectivity for their respective primary target cytokines, which are hIL-6 and hTNFα, over the structurally and functionally related non-primary targets, hIL-11 and hTNFβ. These MM-PBSA analysis provide valuable interaction insights of scFv with cytokines but further experimental validations are required to authenticate the data.

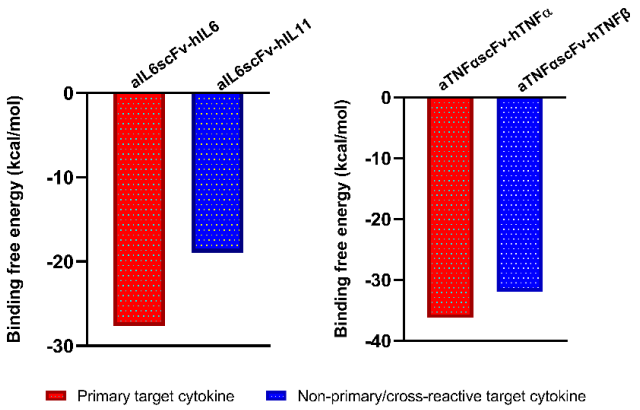


**Figure 0.21** MM-PBSA analysis of scFv-cytokine complexes shows better binding efficiency with primary target

## CONCLUSION

SARS-CoV2 has reminded us of the critical role of an effective host immune response and the devastating effect of immune dysregulation. One of the major causes of the very high mortality rate during this pandemic was assumed to be the cytokine storm. It is potentially a life-threatening condition characterised by the overproduction of inflammatory cytokines, primarily, IL-6 and TNF-α **(Simant & Venkataraman, 2022)**. Presently, the first line of treatment is broad spectrum corticosteroids which are a good immunosuppressive agent. But this immune suppression can lead to various secondary conditions such as allergic reactions, asthma and anaphylactic shocks. This study proposes that the scFv may be a very good alternative to the present treatment and overcome the negative side effects in case of hyper immune response due to various factors. scFv is a great molecule for various reasons such as excellent tissue penetration, low negative immune response, etc. but one of the major benefits is that it is highly specific towards its target which is inferred computationally in this paper. This study has employed protein-protein docking and MD simulations to investigate the binding interaction, stability and dynamic behaviour of murine anti-IL-6 scFv and anti-TNF-α scFv with their primary targets, which are human IL-6 and human TNF-α, respectively. The cross-reactivity of the scFv was also examined with the structurally related cytokines from the same cytokine family, IL-11 and TNF-β. The comprehensive and structural dynamic analysis revealed that the scFv shows more stable and efficient binding with their primary targets and shows very less cross-reactivity. The scFv with its primary target shows high stability, evidenced by low RMSD, high compactness determined by Rg, robust H-bonds network and reduced flexibility claimed by RMSF data. These in-silico findings predict the high specificity of scFv with their primary target. The observed differences in stability and flexibility highlight the importance of optimizing the scFv designs to minimize the off-target interactions, which will eventually enhance the therapeutic efficacy and reduce potential negative side effects.

The present work is based exclusively on computational modelling, docking, molecular dynamics simulations and binding free energy analysis. Although these methods provide valuable structural insight, experimental validation such as ELISA, SPR (Surface Plasmon Resonance), or cell-based neutralization assays are required to confirm biological activity and binding specificity.

**Acknowledgements:** The authors would like to thank VIT University for providing the infrastructure to work.

**Declaration:** The authors declare no conflict of interest.

**Funding:** No funds, grants, or other financial support was received for conducting this study.

## REFERENCES

Abanades, B., Wong, W. K., Boyles, F., Georges, G., Bujotzek, A., & Deane, C. M. (2023). ImmuneBuilder: Deep-Learning models for predicting the structures of immune proteins. *Communications Biology 2023 6:1*, *6*(1), 1–8. https://doi.org/10.1038/s42003-023-04927-7

Abraham, M. J., Murtola, T., Schulz, R., Páll, S., Smith, J. C., Hess, B., & Lindah, E. (2015). GROMACS: High performance molecular simulations through multi-level parallelism from laptops to supercomputers. *SoftwareX*, *1–2*, 19–25. https://doi.org/https://doi.org/10.1016/j.softx.2015.06.001

Abramson, J., Adler, J., Dunger, J., Evans, R., Green, T., Pritzel, A., Ronneberger, O., Willmore, L., Ballard, A. J., Bambrick, J., Bodenstein, S. W., Evans, D. A., Hung, C. C., O'Neill, M., Reiman, D., Tunyasuvunakool, K., Wu, Z., Žemgulytė, A., Arvaniti, E., … Jumper, J. M. (2024). Accurate structure prediction of biomolecular interactions with AlphaFold 3. *Nature*, *630*(8016), 493–500. https://doi.org/https://doi.org/10.1038/s41586-024-07487-w

Ahmad, Z. A., Yeap, S. K., Ali, A. M., Ho, W. Y., Alitheen, N. B. M., & Hamid, M. (2012). ScFv antibody: Principles and clinical application. *Clinical and Developmental Immunology*, *2012*. https://doi.org/doi:10.1155/2012/980250

Aier, I., Varadwaj, P. K., & Raj, U. (2016). Structural insights into conformational stability of both wild-type and mutant EZH2 receptor. *Scientific Reports 2016 6:1*, *6*(1), 34984-. https://doi.org/10.1038/srep34984

AlAjmi, M. F., Khan, S., Choudhury, A., Mohammad, T., Noor, S., Hussain, A., Lu, W., Eapen, M. S., Chimankar, V., Hansbro, P. M., Sohal, S. S., Elasbali, A. M., & Hassan, M. I. (2021). Impact of Deleterious Mutations on Structure, Function and Stability of Serum/Glucocorticoid Regulated Kinase 1: A Gene to Diseases Correlation. *Frontiers in Molecular Biosciences*, *8*, 780284. https://doi.org/10.3389/fmolb.2021.780284

AlphaFold Server. (2024, May). *AlphaFold Server*. Https://Alphafoldserver.Com/Output-Terms. https://alphafoldserver.com/output-terms

Ayub, F., Ahmed, H., Sohail, T., Shahzad, K., Celik, F., Wang, X., Simsek, S., & Cao, J. (2023). Bioinformatics-based prediction and screening of immunogenic epitopes of Toxoplasma gondii rhoptry proteins 7, 21 and 22 as candidate vaccine target. *Heliyon*, *9*(7), e18176. https://doi.org/10.1016/J.HELIYON.2023.E18176

Bhale, A. S., & Venkataraman, K. (2023). Delineating the impact of pathogenic mutations on the conformational dynamics of HDL's vital protein ApoA1: a combined computational and molecular dynamic simulation approach. *Journal of Biomolecular Structure and Dynamics*, *41*(24), 15661–15681. https://doi.org/10.1080/07391102.2023.2191131

Bridger, G. J., Abrams, M. J., Padmanabhan, S., Gaul, F., Larsen, S., Henson, G. W., Schwartz, D. A., Longley, C. B., Burton, C. A., & Ultee, M. E. (1996). A comparison of cleavable and noncleavable hydrazinopyridine linkers for the 99mTc labeling of Fab' monoclonal antibody fragments. *Bioconjugate Chemistry*, *7*(2), 255–264. https://doi.org/10.1021/BC960008R

Choudhury, A., Mohammad, T., Samarth, N., Hussain, A., Rehman, M. T., Islam, A., Alajmi, M. F., Singh, S., & Hassan, M. I. (2021). Structural genomics approach to investigate deleterious impact of nsSNPs in conserved telomere maintenance component 1. *Scientific Reports 2021 11:1*, *11*(1), 1–13. https://doi.org/10.1038/s41598-021-89450-7

Colovos, C., & Yeates, T. O. (1993). Verification of protein structures: patterns of nonbonded atomic interactions. *Protein Science : A Publication of the Protein Society*, *2*(9), 1511–1519. https://doi.org/10.1002/PRO.5560020916

Dai, K., Zhu, H., & Ruan, C. (2003). Generation and characterization of recombinant single chain Fv antibody that recognizes platelet glycoprotein Ibα. *Thrombosis Research*, *109*(2–3), 137–144. https://doi.org/10.1016/S0049-3848(03)00152-X

Debroy, B., Chowdhury, S., & Pal, K. (2023). Designing a novel and combinatorial multi-antigenic epitope-based vaccine "MarVax" against Marburg virus—a reverse vaccinology and immunoinformatics approach. *Journal of Genetic Engineering and Biotechnology*, *21*(1), 143. https://doi.org/10.1186/S43141-023-00575-W

Dunbar, J., Krawczyk, K., Leem, J., Marks, C., Nowak, J., Regep, C., Georges, G., Kelm, S., Popovic, B., & Deane, C. M. (2016). SAbPred: a structure-based antibody prediction server. *Nucleic Acids Research*, *44*(W1), W474–W478. https://doi.org/10.1093/NAR/GKW361

Elrashedy, A., Nayel, M., Salama, A., Salama, M. M., & Hasan, M. E. (2024). Bioinformatics approach for structure modeling, vaccine design, and molecular docking of Brucella candidate proteins BvrR, OMP25, and OMP31. *Scientific Reports*, *14*(1). https://doi.org/10.1038/S41598-024-61991-7

Galeffi, P., Lombardi, A., Pietraforte, I., Novelli, F., Di Donato, M., Sperandei, M., Tornambé, A., Fraioli, R., Martayan, A., Natali, P. G., Benevolo, M., Mottolese, M., Ylera, F., Cantale, C., & Giacomini, P. (2006). Functional expression of a single-chain antibody to ErbB-2 in plants and cell-free systems. *Journal of Translational Medicine*, *4*, 39. https://doi.org/10.1186/1479-5876-4-39

Genheden, S., & Ryde, U. (2015). The MM/PBSA and MM/GBSA methods to estimate ligand-binding affinities. *Expert Opinion on Drug Discovery*, *10*(5), 449–461. https://doi.org/10.1517/17460441.2015.1032936

Ghani, S., Eyvazi, S., Ebrahimi, Z., Bandehpour, M., Ghani, S., Eyvazi, S., Ebrahimi, Z., Bandehpour, M., Ghani, S., Eyvazi, S., Ebrahimi, Z., Bandehpour, M., Ghani, S., Eyvazi, S., Ebrahimi, Z., Bandehpour, M., Ghani, S., Eyvazi, S., Ebrahimi, Z., … Bandehpour, M. (2023). In Silico Evaluation of the Interactions Among Novel Phage Display-Selected Single Chain Variable Fragment (scFv) with CD24 Marker. *International Journal of Cancer Management 2023 16:1*, *16*(1), e136917. https://doi.org/10.5812/IJCM-136917

Goddard, T. D., Brilliant, A. A., Skillman, T. L., Vergenz, S., Tyrwhitt-Drake, J., Meng, E. C., & Ferrin, T. E. (2018). Molecular Visualization on the Holodeck. *Journal of Molecular Biology*, *430*(21), 3982–3996. https://doi.org/10.1016/j.jmb.2018.06.040

Goddard, T. D., Huang, C. C., & Ferrin, T. E. (2005). Software extensions to UCSF chimera for interactive visualization of large molecular assemblies. *Structure*, *13*(3), 473–482. https://doi.org/10.1016/j.str.2005.01.006

Green, L. L. (1999). Antibody engineering via genetic engineering of the mouse: XenoMouse strains are a vehicle for the facile generation of therapeutic human monoclonal antibodies. *Journal of Immunological Methods*, *231*(1–2), 11–23. https://doi.org/10.1016/S0022-1759(99)00137-4

Guex, N., Peitsch, M. C., & Schwede, T. (2009). Automated comparative protein structure modeling with SWISS-MODEL and Swiss-PdbViewer: A historical perspective. *ELECTROPHORESIS*, *30*(S1), S162–S173. https://doi.org/10.1002/ELPS.200900140

He, J., Zhou, G., Liu, K. Da, & Qin, X. Y. (2002). Construction and preliminary screening of a human phage single-chain antibody library associated with gastric cancer. *Journal of Surgical Research*, *102*(2), 150–155. https://doi.org/10.1006/jsre.2001.6298

Ho, B. K., & Brasseur, R. (2005). The Ramachandran plots of glycine and pre-proline. *BMC Structural Biology*, *5*(1), 1–11. https://doi.org/10.1186/1472-6807-5-14/TABLES/1

Holliger, P., & Hudson, P. J. (2005). Engineered antibody fragments and the rise of single domains. *Nature Biotechnology*, *23*(9), 1126–1136. https://doi.org/10.1038/NBT1142

Hollingsworth, S. A., & Karplus, P. A. (2010). A fresh look at the Ramachandran plot and the occurrence of standard structures in proteins. *Biomolecular Concepts*, *1*(3–4), 271–283. https://doi.org/10.1515/BMC.2010.022/PDF

Honorato, R. V., Koukos, P. I., Jiménez-García, B., Tsaregorodtsev, A., Verlato, M., Giachetti, A., Rosato, A., & Bonvin, A. M. J. J. (2021). Structural Biology in the Clouds: The WeNMR-EOSC Ecosystem. *Frontiers in Molecular Biosciences*, *8*, 729513. https://doi.org/10.3389/fmolb.2021.729513

Honorato, R. V., Trellet, M. E., Jiménez-García, B., Schaarschmidt, J. J., Giulini, M., Reys, V., Koukos, P. I., Rodrigues, J. P. G. L. M., Karaca, E., van Zundert, G. C. P., Roel-Touris, J., van Noort, C. W., Jandová, Z., Melquiond, A. S. J., & Bonvin, A. M. J. J. (2024). The HADDOCK2.4 web server for integrative modeling of biomolecular complexes. *Nature Protocols 2024 19:11*, *19*(11), 3219–3241. https://doi.org/10.1038/s41596-024-01011-0

Hu, B., Huang, S., & Yin, L. (2021). The cytokine storm and COVID-19. *Journal of Medical Virology*, *93*(1), 250–256. https://doi.org/10.1002/JMV.26232

Jarasch, A., Koll, H., Regula, J. T., Bader, M., Papadimitriou, A., & Kettenberger, H. (2015). Developability Assessment During the Selection of Novel Therapeutic Antibodies. *Journal of Pharmaceutical Sciences*, *104*(6), 1885–1898. https://doi.org/10.1002/JPS.24430

Kantarjian, H., Stein, A., Gökbuget, N., Fielding, A. K., Schuh, A. C., Ribera, J.-M., Wei, A., Dombret, H., Foà, R., Bassan, R., Arslan, Ö., Sanz, M. A., Bergeron, J., Demirkan, F., Lech-Maranda, E., Rambaldi, A., Thomas, X., Horst, H.-A., Brüggemann, M., … Topp, M. S. (2017). Blinatumomab versus Chemotherapy for Advanced Acute Lymphoblastic Leukemia. *New England Journal of Medicine*, *376*(9), 836–847. https://doi.org/10.1056/NEJMoa1609783

Keskin, O. (2007). Binding induced conformational changes of proteins correlate with their intrinsic fluctuations: a case study of antibodies. *BMC Structural Biology 2007 7:1*, *7*(1), 31-. https://doi.org/10.1186/1472-6807-7-31

Khetan, R., Curtis, R., Deane, C. M., Hadsund, J. T., Kar, U., Krawczyk, K., Kuroda, D., Robinson, S. A., Sormanni, P., Tsumoto, K., Warwicker, J., & Martin, A. C. R. (2022). Current advances in biopharmaceutical informatics: guidelines, impact and challenges in the computational developability assessment of antibody therapeutics. *MAbs*, *14*(1). https://doi.org/10.1080/19420862.2021.2020082

Kobayashi, N., Ohtoyo, M., Wada, E., Kato, Y., Mano, N., & Goto, J. (2005). Generation of a single-chain Fv fragment for the monitoring of deoxycholic acid residues anchored on endogenous proteins. *Steroids*, *70*(4), 285–294. https://doi.org/10.1016/J.STEROIDS.2004.11.012

Krieger, E., Joo, K., Lee, J., Lee, J., Raman, S., Thompson, J., Tyka, M., Baker, D., & Karplus, K. (2009). Improving physical realism, stereochemistry, and side-chain accuracy in homology modeling: Four approaches that performed well in CASP8. *Proteins: Structure, Function, and Bioinformatics*, *77*(S9), 114–122. https://doi.org/10.1002/PROT.22570

Kurniawan, J., & Ishida, T. (2022). Protein Model Quality Estimation Using Molecular Dynamics Simulation. *ACS Omega*, *7*(28), 24274–24281. https://doi.org/10.1021/ACSOMEGA.2C01475

Laskowski, R. A., MacArthur, M. W., Moss, D. S., & Thornton, J. M. (1993). PROCHECK: a program to check the stereochemical quality of protein structures. *Journal of Applied Crystallography*, *26*(2), 283–291. https://doi.org/https://doi.org/10.1107/S0021889892009944

Laskowski, R. A., Rullmann, J. A. C., MacArthur, M. W., Kaptein, R., & Thornton, J. M. (1996). AQUA and PROCHECK-NMR: Programs for checking the quality of protein structures solved by NMR. *Journal of Biomolecular NMR*, *8*(4), 477–486. https://doi.org/10.1007/BF00228148,

Lindahl, E., Bjelkmar, P., Larsson, P., Cuendet, M. A., & Hess, B. (2010). Implementation of the CHARMM Force Field in GROMACS: Analysis of Protein Stability Effects from Correction Maps, Virtual Interaction Sites, and Water Models. *Journal of Chemical Theory and Computation*, *6*(2), 459–466. https://doi.org/10.1021/CT900549R

Liu, C., Denzler, L. M., Hood, O. E. C., & Martin, A. C. R. (2024). Do antibody CDR loops change conformation upon binding? *MAbs*, *16*(1), 2322533. https://doi.org/10.1080/19420862.2024.2322533

Martarelli, N., Capurro, M., Mansour, G., Jahromi, R. V., Stella, A., Rossi, R., Longetti, E., Bigerna, B., Gentili, M., Rosseto, A., Rossi, R., Cencini, C., Emiliani, C., Martino, S., Beeg, M., Gobbi, M., Tiacci, E., Falini, B., Morena, F., & Perriello, V. M. (2024a). Artificial Intelligence-Powered Molecular Docking and Steered Molecular Dynamics for Accurate scFv Selection of Anti-CD30 Chimeric Antigen Receptors. *International Journal of Molecular Sciences*, *25*(13), 7231. https://doi.org/10.3390/IJMS25137231/S1

Martarelli, N., Capurro, M., Mansour, G., Jahromi, R. V., Stella, A., Rossi, R., Longetti, E., Bigerna, B., Gentili, M., Rosseto, A., Rossi, R., Cencini, C., Emiliani, C., Martino, S., Beeg, M., Gobbi, M., Tiacci, E., Falini, B., Morena, F., & Perriello, V. M. (2024b). Artificial Intelligence-Powered Molecular Docking and Steered Molecular Dynamics for Accurate scFv Selection of Anti-CD30 Chimeric Antigen Receptors. *International Journal of Molecular Sciences*, *25*(13), 7231. https://doi.org/10.3390/IJMS25137231/S1

Muñoz-López, P., Ribas-Aparicio, R. M., Becerra-Báez, E. I., Fraga-Pérez, K., Flores-Martínez, L. F., Mateos-Chávez, A. A., & Luria-Pérez, R. (2022). Single-Chain Fragment Variable: Recent Progress in Cancer Diagnosis and Therapy. *Cancers*, *14*(17). https://doi.org/10.3390/cancers14174206

Muyldermans, S. (2013). Nanobodies: natural single-domain antibodies. *Annual Review of Biochemistry*, *82*, 775–797. https://doi.org/10.1146/annurev-biochem-063011-092449

Okazaki, K., Kobashigawa, Y., Morita, H., Yamauchi, S., Fukuda, N., Liu, C., Toyota, Y., Sato, T., & Morioka, H. (2023). Molecular Dynamics-Based Design and Biophysical Evaluation of Thermostable Single-Chain Fv Antibody Mutants Derived from Pharmaceutical Antibodies. *ACS Omega*, *8*(25), 22945–22954. https://doi.org/10.1021/ACSOMEGA.3C01948

Pettersen, E. F., Goddard, T. D., Huang, C. C., Meng, E. C., Couch, G. S., Croll, T. I., Morris, J. H., & Ferrin, T. E. (2021). UCSF ChimeraX: Structure visualization for researchers, educators, and developers. *Protein Science*, *30*(1), 70–82. https://doi.org/10.1002/PRO.3943,

Pourtaghi-Anvarian, S., Mohammadi, S., Hamzeh-Mivehroud, M., Alizadeh, A. A., & Dastmalchi, S. (2019). Characterization of the novel anti-TNF-α single-chain fragment antibodies using experimental and computational approaches. *Preparative Biochemistry and Biotechnology*, *49*(1), 38–47. https://doi.org/10.1080/10826068.2018.1487855

Powell, H. R., Islam, S. A., David, A., & Sternberg, M. J. E. (2025). Phyre2.2: A Community Resource for Template-based Protein Structure Prediction. *Journal of Molecular Biology*, 168960. https://doi.org/10.1016/J.JMB.2025.168960

Ravn, P., Danielczyk, A., Bak Jensen, K., Kristensen, P., Astrup Christensen, P., Larsen, M., Karsten, U., & Goletz, S. (2004). Multivalent scFv Display of Phagemid Repertoires for the Selection of Carbohydrate-specific Antibodies and its Application to the Thomsen–Friedenreich Antigen. *Journal of Molecular Biology*, *343*(4), 985–996. https://doi.org/10.1016/J.JMB.2004.08.052

Rezaei Adriani, R., Mousavi Gargari, S. L., Bakherad, H., & Amani, J. (2024). In silico designing and optimization of anti-epidermal growth factor receptor scaffolds by complementary-determining regions-grafting technique. *Quantitative Biology*, *12*(3), 301. https://doi.org/10.1002/QUB2.63

Richard, A. C., & Pantazes, R. J. (2025). Using Short Molecular Dynamics Simulations to Determine the Important Features of Interactions in Antibody–Protein Complexes. *Proteins: Structure, Function, and Bioinformatics*, *93*(4), 812–830. https://doi.org/10.1002/PROT.26773

Safarpour, H., Shahmirzaie, M., Rezaee, E., Barati, M., Safarnejad, M. R., & Shirazi, F. H. (2018). Isolation and Characterization of Novel Phage Displayed scFv Fragment for Human Tumor Necrosis Factor Alpha and Molecular Docking Analysis of Their Interactions. In *Iranian Journal of Pharmaceutical Research* (Vol. 17, Number 2).

Schreiner, W., Karch, R., Knapp, B., & Ilieva, N. (2012). Relaxation Estimation of RMSD in Molecular Dynamics Immunosimulations. *Computational and Mathematical Methods in Medicine*, *2012*, 173521. https://doi.org/10.1155/2012/173521

Scott, A. M., Wolchok, J. D., & Old, L. J. (2012). Antibody therapy of cancer. *Nature Reviews Cancer 2012 12:4*, *12*(4), 278–287. https://doi.org/10.1038/nrc3236

Simant, K., & Venkataraman, K. (2022). Interleukin-6, a major player of cytokine storm in COVID-19 and its alleviation by therapeutic antibodies. *Current Science*, *123*(6), 745–753. https://doi.org/10.18520/cs/v123/i6/745-753

Srivastava, V. K., Kaushik, S., Bhargava, G., Jain, A., Saxena, J., & Jyoti, A. (2021). A Bioinformatics Approach for the Prediction of Immunogenic Properties and Structure of the SARS-COV-2 B.1.617.1 Variant Spike Protein. *BioMed Research International*, *2021*, 7251119. https://doi.org/10.1155/2021/7251119

Thomas, J., Kumar, S., & Satija, J. (2024). Integrated molecular and quantum mechanical approach to identify novel potent natural bioactive compound against 2′-O-methyltransferase (nsp16) of SARS-CoV-2. *Journal of Biomolecular Structure and Dynamics*, *42*(4), 1999–2012. https://doi.org/10.1080/07391102.2023.2206287

Thomas, J., & Satija, J. (2024). Cheminformatics and QSAR-Based Identification of Natural Bioactive Compounds as Potent Inhibitors of SARS-CoV-2 N-7 Methyltransferases. *ChemistrySelect*, *9*(17). https://doi.org/10.1002/slct.202304932

Wang, T., & Duan, Y. (2011). Probing the stability-limiting regions of an antibody single-chain variable fragment: a molecular dynamics simulation study. *Protein Engineering, Design and Selection*, *24*(9), 649. https://doi.org/10.1093/PROTEIN/GZR029

Wang, Z., Li, J., Wang, M., Yu, Y., Lu, Y., Xia, Q., & Wei, P. (2025). Reconciling specificity and non-specificity in antibody binding: an energy landscape framework for immunology education. *Frontiers in Immunology*, *16*, 1650722. https://doi.org/10.3389/FIMMU.2025.1650722

Waterhouse, A., Bertoni, M., Bienert, S., Studer, G., Tauriello, G., Gumienny, R., Heer, F. T., De Beer, T. A. P., Rempfer, C., Bordoli, L., Lepore, R., & Schwede, T. (2018). SWISS-MODEL: homology modelling of protein structures and complexes. *Nucleic Acids Research*, *46*(W1), W296–W303. https://doi.org/10.1093/NAR/GKY427

Xue, L., Yi, Y., Xu, Q., Wang, L., Yang, X., Zhang, Y., Hua, X., Chai, X., Yang, J., Chen, Y., Tao, G., Hu, B., & Wang, X. (2021). Chimeric antigen receptor T cells self-neutralizing IL6 storm in patients with hematologic malignancy. *Cell Discovery*, *7*(1), 1–15. https://doi.org/https://doi.org/10.1038/s41421-021-00299-6

Yaghoobizadeh, F., Roayaei Ardakani, M., Ranjbar, M. M., Khosravi, M., & Galehdari, H. (2024). Development of a potent recombinant scFv antibody against the SARS-CoV-2 by in-depth bioinformatics study: Paving the way for vaccine/diagnostics development. *Computers in Biology and Medicine*, *170*. https://doi.org/10.1016/j.compbiomed.2024.108091

Yang, J., & Zhang, Y. (2015). I-TASSER server: new development for protein structure and function predictions. *Web Server Issue Published Online*, *43*. https://doi.org/10.1093/nar/gkv342

Yiu, H. H., Graham, A. L., & Stengel, R. F. (2012). Dynamics of a Cytokine Storm. *PLOS ONE*, *7*(10), e45027. https://doi.org/10.1371/JOURNAL.PONE.0045027

Yoshida, K., Kuroda, D., Kiyoshi, M., Nakakido, M., Nagatoishi, S., Soga, S., Shirai, H., & Tsumoto, K. (2019). Exploring designability of electrostatic complementarity at an antigen-antibody interface directed by mutagenesis, biophysical analysis, and molecular dynamics simulations. *Scientific Reports 2019 9:1*, *9*(1), 4482-. https://doi.org/10.1038/s41598-019-40461-5

Zhang, H., Zhu, L., Zou, E., Liang, Y., Zou, L., & Biotech, K. (2023). Development of a method for producing FAb/F(Ab')2 fragments from a full-length monoclonal antibody for bioanalytical assays. *Antibody Therapeutics*, *6*(Suppl 1), tbad014.019. https://doi.org/10.1093/ABT/TBAD014.019

Zhou, X., Zheng, W., Li, Y., Pearce, R., Zhang, C., Bell, E. W., Zhang, G., & Zhang, Y. (2022). I-TASSER-MTD: a deep-learning-based platform for multi-domain protein structure and function prediction. *Nature Protocols*, *17*(10), 2326–2353. https://doi.org/10.1038/S41596-022-00728-0,